CHAPTER 6

CHAPTER 7

CHAPTER 5
Inertial Navigation

An inertial navigation system (INS), sometimes known as an inertial navigation unit (INU), is an example of a dead-reckoning navigation system. A position solution is maintained by integrating velocity, which, in turn, is maintained by integrating acceleration measurements obtained using an IMU. An attitude solution is also maintained by integrating the IMU's angular rate measurements. Following initialization, navigation can proceed without further information from the environment. Hence, inertial navigation systems are self-contained.

Inertial navigation has been used since the 1960s and 1970s for applications such as civil aviation, military aviation, submarines, military ships, and guided weapons. Some historical notes may be found in Section E.4 of Appendix E on the CD. These systems can typically operate either stand-alone or as part of an integrated navigation system. For newer applications, such as light aircraft, helicopters, unmanned air vehicles (UAVs), land vehicles, mobile mapping, and pedestrians, low-cost sensors are typically used and inertial navigation forms part of an INS/GNSS or multisensor integrated navigation system (Chapters 14 and 16).

As shown in Figure 5.1, an INS comprises an inertial measurement unit and a navigation processor. The IMU, described in the previous chapter, measures specific force and angular rate using a set of accelerometers and gyros. The discussion of IMU grades in Chapter 4 also applies to the INS as a whole. The navigation processor may be packaged with the IMU and the system sold as a complete INS. Alternatively, the navigation equations may be implemented on an integrated navigation processor or on the application's central processor. Marine, aviation, and intermediate grade inertial sensors tend to be sold as part of an INS, while tactical grade inertial sensors are usually sold as an IMU. In either case, the function is the same, so the term inertial navigation system is applied here to all architectures in which a three-dimensional navigation solution is obtained from inertial sensor measurements.

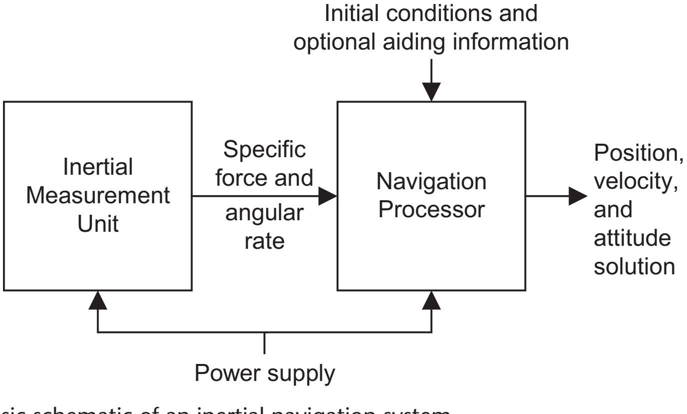
Initial conditions and optional aiding information
Inertial Measurement Unit
Specific force and angular rate
Navigation Processor
Position, velocity, and attitude solution
Power supply

Figure 5.1 Basic schematic of an inertial navigation system.

This chapter focuses on the navigation processor. Section 5.1 introduces the main concepts of inertial navigation, illustrated by simple one- and two-dimensional examples. Three-dimensional navigation equations are then presented in Sections 5.2 to 5.5. A strapdown configuration, whereby the inertial sensors are fixed with respect to the vehicle body, is assumed throughout this chapter. The alternative platform configuration is described in Section E.5 of Appendix E on the CD.

Computation of an inertial navigation solution is an iterative process, making use of the solution from the previous iteration. Therefore, the navigation solution must be initialized before the INS can function. Section 5.6 describes the different methods of initializing the position, velocity, and attitude, including self-alignment and fine alignment processes.

Section 5.7 describes the error behavior of an INS. Errors can arise from the IMU, the initialization process, and the navigation equations. These then propagate through the navigation equations to give position, velocity, and attitude errors that vary with time. The short-term and long-term cases are examined. Finally, Section 5.8 discusses indexing, used to increase accuracy on ships and submarines, and Section 5.9 discusses inertial navigation using a partial IMU. Appendix E on the CD provides further information on a number of topics. A MATLAB inertial navigation simulation is also included on the accompanying CD.

Note that this chapter builds on the mathematical foundations introduced in Chapter 2.

5.1 Introduction to Inertial Navigation

An example of single-dimensional inertial navigation is considered first. A body, b, is constrained to move with respect to an Earth-fixed reference frame, p, in a straight line perpendicular to the direction of gravity. The body's axes are fixed with respect to frame p, so its motion has only one degree of freedom. Its Earth-referenced acceleration may be measured by a single accelerometer with its sensitive axis aligned along the direction of motion (neglecting the Coriolis force).

If the speed, v_{pb}, is known at an earlier time, t_0, it may be determined at a later time, t, simply by integrating the acceleration, a_{pb}:

$$v_{pb}(t) = v_{pb}(t_0) + \int_{t_0}^{t} a_{pb}(t')\,dt'. \tag{5.1}$$

Similarly, if the position, r_{pb}, at time t_0 is known, its value at time t may be obtained by integrating the velocity:

$$\begin{aligned} r_{pb}(t) &= r_{pb}(t_0) + \int_{t_0}^{t} v_{pb}(t')\,dt' \\ &= r_{pb}(t_0) + (t - t_0)v_{pb}(t_0) + \int_{t_0}^{t}\int_{t_0}^{t'} a_{pb}(t'')\,dt''\,dt' \end{aligned} . \tag{5.2}$$

Extending the example to two dimensions, the body is now constrained to move within a horizontal plane defined by the x and y axes of the p frame. It may be oriented in any direction within this plane, but is constrained to remain level. It thus has one angular and two linear degrees of freedom. By analogy with the one-dimensional example, the position and velocity, resolved along the axes of the reference frame, p, are updated using

$$\begin{pmatrix} v^p_{pb,x}(t) \\ v^p_{pb,y}(t) \end{pmatrix} = \begin{pmatrix} v^p_{pb,x}(t_0) \\ v^p_{pb,y}(t_0) \end{pmatrix} + \int_{t_0}^{t} \begin{pmatrix} a^p_{pb,x}(t') \\ a^p_{pb,y}(t') \end{pmatrix} dt', \tag{5.3}$$

$$\begin{pmatrix} x^p_{pb}(t) \\ y^p_{pb}(t) \end{pmatrix} = \begin{pmatrix} x^p_{pb}(t_0) \\ y^p_{pb}(t_0) \end{pmatrix} + \int_{t_0}^{t} \begin{pmatrix} v^p_{pb,x}(t') \\ v^p_{pb,y}(t') \end{pmatrix} dt'. \tag{5.4}$$

Two accelerometers are required to measure the acceleration along two orthogonal axes. However, their sensitive axes will be aligned with those of the body, b. To determine the acceleration along the axes of frame p, the heading of frame b with respect to frame p, ψ_{pb}, is required. Figure 5.2 illustrates this. The rotation of the body with respect to the reference frame may be measured with a single gyro sensitive to rotation in the horizontal plane (neglecting Earth rotation). Thus, three inertial sensors are required to measure the three degrees of freedom of motion in two dimensions.

If the heading, ψ_{pb}, is known at the earlier time, t_0, it may be determined at the later time, t, by integrating the angular rate, $\omega^b_{pb,z}$:

$$\psi_{pb}(t) = \psi_{pb}(t_0) + \int_{t_0}^{t} \omega^b_{pb,z}(t')\, dt'. \tag{5.5}$$

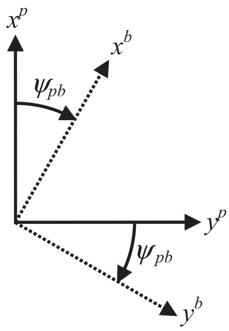

Figure 5.2 Orientation of body axes with respect to the resolving axes in a horizontal plane.

The accelerometer measurements may be transformed to the p-frame resolving axes using a 2×2 coordinate transformation matrix:

$$\begin{pmatrix} a^{p}_{pb,x}(t') \\ a^{p}_{pb,y}(t') \end{pmatrix} = \begin{pmatrix} \cos\psi_{pb}(t') & -\sin\psi_{pb}(t') \\ \sin\psi_{pb}(t') & \cos\psi_{pb}(t') \end{pmatrix} \begin{pmatrix} a^{b}_{pb,x}(t') \\ a^{b}_{pb,y}(t') \end{pmatrix}. \tag{5.6}$$

There is a clear dependency in processing the equations. The heading update must be computed before the accelerometer-output resolving frame transformation; the frame transformation must be computed before the velocity update; and the velocity update must be computed before the position update. Example 5.1 on the CD illustrates this over four measurement epochs and is editable using Microsoft Excel.

These one- and two-dimensional examples are presented only to aid understanding of the concepts of inertial navigation. For all practical applications, including ships, trains, and road vehicles, three-dimensional motion must be assumed. Although land and marine navigation is essentially a two-dimensional problem, strapdown inertial sensors will not remain in the horizontal plane due to terrain slopes or ship pitching and rolling. If the accelerometers are not in the horizontal plane, they will sense the reaction to gravity as well as the horizontal-plane acceleration. A platform tilt of just 10 mrad (0.57°) will produce an acceleration error of 0.1 m s^{-2}. If this is sustained for 100 seconds, the velocity error will be 10 m s^{-1} and the position error will be 500m. Tilts of 10 times this are quite normal for both cars and boats.

Motion in three dimensions generally has six degrees of freedom: three linear and three angular. Thus, six inertial sensors are required to measure that motion. A full strapdown IMU produces measurements of the specific force, $\mathbf{f}^{b}_{ib}$, and angular rate, $\boldsymbol{\omega}^{b}_{ib}$, of the IMU body frame with respect to inertial space in body-frame axes. Motion is *not* measured with respect to the Earth. Integrated specific force, $\boldsymbol{\upsilon}^{b}_{ib}$, and attitude increments, $\boldsymbol{\alpha}^{b}_{ib}$, may be output as an alternative. In general, none of the accelerometers may be assumed to be measuring pure acceleration. Therefore, a model of the gravitational acceleration must be used to determine inertially-referenced acceleration from the specific force measurements, while a gravity model must be used to obtain Earth-referenced acceleration (see Section 2.4.7).

Figure 5.3 shows a schematic of an inertial navigation processor. The IMU outputs are integrated to produce an updated position, velocity, and attitude solution in four steps:

1. The attitude update;
2. The transformation of the specific-force resolving axes from the IMU body frame to the coordinate frame used to resolve the position and velocity solutions;
3. The velocity update, including transformation of specific force into acceleration using a gravity or gravitation model;
4. The position update.

In an integrated navigation system, there may also be correction of the IMU outputs and the inertial navigation solution using estimates from the integration algorithm (see Section 14.1.1).

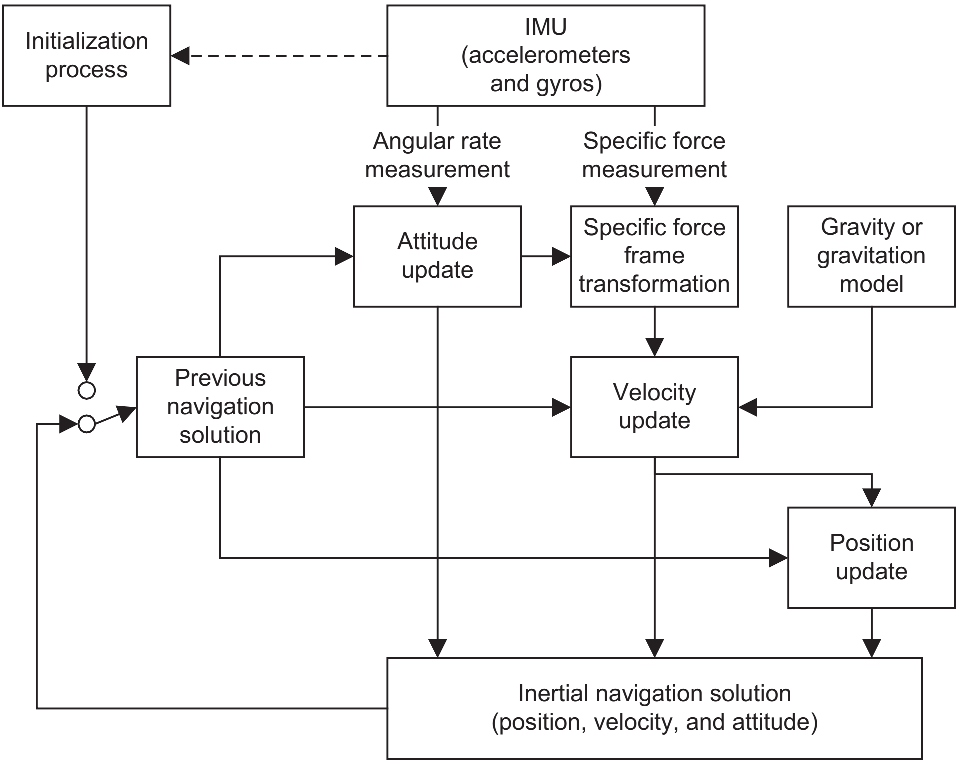
Initialization process
IMU (accelerometers and gyros)
Angular rate measurement
Specific force measurement
Attitude update
Specific force frame transformation
Gravity or gravitation model
Previous navigation solution
Velocity update
Position update
Inertial navigation solution (position, velocity, and attitude)

Figure 5.3 Schematic of an inertial navigation processor.

The form of the inertial navigation equations, also known as the strapdown computation, depends on the choice of reference frame and resolving axes (see Section 2.1). Section 5.2 describes the navigation equations for an Earth-centered inertial frame implementation, while Section 5.3 describes how they are modified for implementation in a rotating Earth-centered Earth-fixed frame. Section 5.4 presents an Earth-referenced local-navigation-frame implementation with curvilinear position. It also discusses the wander-azimuth-frame variant. In addition, Section E.7 of Appendix E on the CD presents a local tangent-plane implementation. Note that the navigation solution may be transformed to a different form for user output as described in Sections 2.4.3 and 2.5.

Continuous-time navigation equations, such as those presented for the one- and two-dimensional examples, physically describe a body's motion. Discrete-time navigation equations, also known as mechanization equations, provide a means of updating a navigation solution over a discrete time interval. They are an approximation of the continuous-time equations. Sections 5.2 to 5.4 present the continuous-time navigation equations together with the simplest practical mechanizations of the discrete-time equations, applying a number of first-order approximations and assuming that all stages are iterated at the IMU output rate. Section 5.5 then describes how the precision and/or efficiency of the inertial navigation equations may be improved and discusses which forms are appropriate for different applications.

As discussed in Section 4.3, the IMU provides outputs of specific force and angular rate averaged or integrated over a discrete sampling interval, τ_i. This provides a natural interval over which to compute each inertial navigation processing cycle.

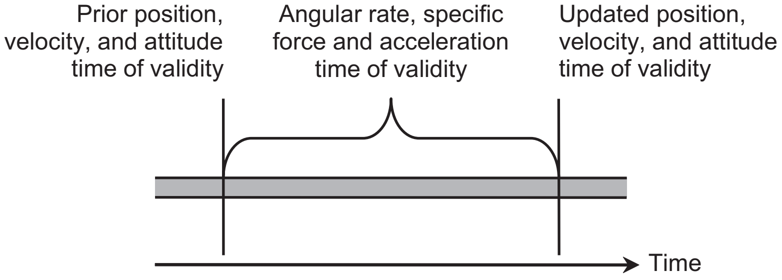
Prior position, velocity, and attitude time of validity
Angular rate, specific force and acceleration time of validity
Updated position, velocity, and attitude time of validity
Time

Figure 5.4 Times of validity of quantities in inertial navigation.

Consequently, this IMU output interval is taken as the time step for the navigation equations presented in Sections 5.2 to 5.4; the use of other time steps is discussed in Section 5.5. The position, velocity, and attitude solution is valid at the end of the IMU sampling interval. Figure 5.4 illustrates this.

Accurate timing is important for inertial navigation. It is needed for correct integration of the velocity to update the position and for integration of the specific force and angular rate, where required. It is also needed for correct transformation between ECI and ECEF resolving and references axes, which is required for all inertial navigation mechanization equations.

All the navigation equations presented in this chapter use the coordinate transformation matrix representation of attitude as this is the clearest. The quaternion form of the attitude update is described in Section E.6.3 of Appendix E on the CD. Navigation equations are also presented in [1, 2].

5.2 Inertial-Frame Navigation Equations

Figure 5.5 shows how the angular-rate and specific-force measurements made over the time interval t to $t + \tau_i$ are used to update the attitude, velocity, and position, expressed with respect to and resolved in the axes of an ECI coordinate frame. Each of the four steps is described in turn. The suffixes (–) and (+) are, respectively, used to denote values at the beginning of the navigation equations processing cycle, at time t, and at the end of the processing cycle, at time $t + \tau_i$. The inertial-frame navigation equations are the simplest of those presented here. However, a frame transformation must be applied to obtain an Earth-referenced solution for user output. Example 5.2 on the CD shows one processing cycle of the approximate navigation equations described in this section and is editable using Microsoft Excel.

5.2.1 Attitude Update

The attitude update step of the inertial navigation equations uses the angular-rate measurement from the IMU, $\boldsymbol{\omega}_{ib}^{b}$, to update the attitude solution, expressed as the body-to-inertial-frame coordinate transformation matrix, $\mathbf{C}_b^i$.

From (2.56), the time derivative of the coordinate transformation matrix is

$$\dot{\mathbf{C}}_b^i = \mathbf{C}_b^i \boldsymbol{\Omega}_{ib}^b \tag{5.7}$$

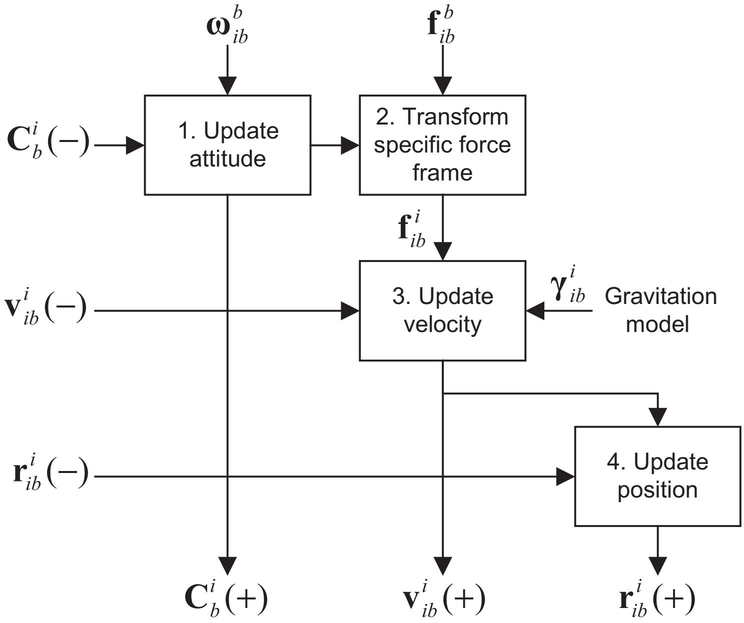

Figure 5.5 Block diagram of ECI-frame navigation equations.

recalling from Section 2.3.1 that $\boldsymbol{\Omega}_{ib}^{b} = \left[\boldsymbol{\omega}_{ib}^{b} \wedge\right]$, the skew-symmetric matrix of the angular rate. Integrating this gives

$$\mathbf{C}_{b}^{i}(t+\tau_{i}) = \mathbf{C}_{b}^{i}(t)\left[\lim_{n\to\infty}\prod_{i=1}^{n}\exp\left(\boldsymbol{\Omega}_{ib}^{b}\left(t+\frac{n-i}{n}\tau_{i}\right)\frac{\tau_{i}}{n}\right)\right], \tag{5.8}$$

noting (A.17) in Appendix A on the CD. If the angular rate is assumed to be constant over the attitude integration interval, this simplifies to

$$\begin{aligned} \mathbf{C}_{b}^{i}(t+\tau_{i}) &\approx \mathbf{C}_{b}^{i}(t)\exp\left(\boldsymbol{\Omega}_{ib}^{b}\tau_{i}\right) \\ &= \mathbf{C}_{b}^{i}(t)\exp\left(\left[\boldsymbol{\omega}_{ib}^{b} \wedge\right]\tau_{i}\right)^{.} \end{aligned} \tag{5.9}$$

This assumption is often made where the attitude integration is performed at the IMU output rate. Applying (4.9), this may be expressed in terms of the attitude increment, $\boldsymbol{\alpha}_{ib}^{b}$:

$$\mathbf{C}_{b}^{i}(t+\tau_{i}) = \mathbf{C}_{b}^{i}(t)\exp\left(\left[\boldsymbol{\alpha}_{ib}^{b} \wedge\right]\right). \tag{5.10}$$

Section 5.5.4 shows how a resultant attitude increment may be summed from successive increments in a way that correctly accounts for the noncommutivity of rotations. Therefore, (5.10) may be either exact or an approximation, depending on how $\boldsymbol{\alpha}_{ib}^{b}$ is calculated.

The exponent of a matrix is not the same as the matrix of the exponents of its components. Expressing (5.10) as a power series,

$$\mathbf{C}_b^i(t+\tau_i) = \mathbf{C}_b^i(t)\sum_{r=0}^{\infty}\frac{\left[\boldsymbol{\alpha}_{ib}^b \wedge\right]^r}{r!}. \tag{5.11}$$

The simplest form of the attitude update is obtained by truncating the power-series expansion to first order:

$$\mathbf{C}_b^i(+) \approx \mathbf{C}_b^i(-)\left(\mathbf{I}_3 + \left[\boldsymbol{\alpha}_{ib}^b \wedge\right]\right). \tag{5.12}$$

When the angular rate is assumed to be constant over the attitude integration interval, $\boldsymbol{\alpha}_{ib}^b \approx \boldsymbol{\omega}_{ib}^b\tau_i$. In this case, (5.12) becomes

$$\mathbf{C}_b^i(+) \approx \mathbf{C}_b^i(-)\left(\mathbf{I}_3 + \boldsymbol{\Omega}_{ib}^b\tau_i\right), \tag{5.13}$$

where

$$\mathbf{I}_3 + \boldsymbol{\Omega}_{ib}^b\tau_i = \begin{pmatrix} 1 & -\omega_{ib,z}^b\tau_i & \omega_{ib,y}^b\tau_i \\ \omega_{ib,z}^b\tau_i & 1 & -\omega_{ib,x}^b\tau_i \\ -\omega_{ib,y}^b\tau_i & \omega_{ib,x}^b\tau_i & 1 \end{pmatrix}. \tag{5.14}$$

This first-order approximation of (5.11) is a form of the small angle approximation, $\sin\theta \approx \theta$, $\cos\theta \approx 1$. The truncation of the power-series introduces errors in the attitude integration that will be larger at lower iteration rates (large τ_i) and higher angular rates. As discussed in Section 5.5.1, these errors are largest where the first-order approximation is used. In practice, the first-order approximation can be used for land vehicle applications where the dynamics are low, but not for high-dynamic applications, such as aviation. It is also unsuited to applications with regular periodic motion, such as pedestrian and boat navigation [3].

Precision may be improved by including higher-order terms in the power series, (5.11), breaking down the attitude update into smaller steps (see Section 5.5.5), or performing the exact attitude update, described in Section 5.5.1. All of these increase the complexity and processor load.

5.2.2 Specific-Force Frame Transformation

The IMU measures specific force along the body-frame resolving axes. However, for use in the velocity integration step of the navigation equations, it must be resolved about the same axes as the velocity—in this case, an ECI frame. The resolving axes are transformed simply by applying a coordinate transformation matrix:

$$\mathbf{f}_{ib}^i(t) = \mathbf{C}_b^i(t)\mathbf{f}_{ib}^b(t). \tag{5.15}$$

As the specific-force measurement is an average over time t to $t + \tau_i$, the coordinate transformation matrix should be similarly averaged. A simple implementation, assuming a constant angular rate, is

$$\mathbf{f}_{ib}^{i} \approx \tfrac{1}{2}\left(\mathbf{C}_{b}^{i}(-) + \mathbf{C}_{b}^{i}(+)\right)\mathbf{f}_{ib}^{b}. \tag{5.16}$$

However, the mean of two coordinate transformation matrices does not precisely produce the mean of the two attitudes. A more accurate form is presented in Section 5.5.2, while Section 5.5.4 shows how to account for variation in the angular rate over the update interval. The less the attitude varies over the time interval, the smaller the errors introduced by this approximation.

When the IMU outputs integrated specific force, this is transformed in the same way:

$$\begin{aligned} \boldsymbol{\upsilon}_{ib}^{i} &= \bar{\mathbf{C}}_{b}^{i}\boldsymbol{\upsilon}_{ib}^{b} \\ &\approx \tfrac{1}{2}\left(\mathbf{C}_{b}^{i}(-) + \mathbf{C}_{b}^{i}(+)\right)\boldsymbol{\upsilon}_{ib}^{b} \end{aligned}, \tag{5.17}$$

where $\bar{\mathbf{C}}_{b}^{i}$ is the average value of the coordinate transformation matrix over the interval from t to $t + \tau_i$.

5.2.3 Velocity Update

As given by (2.125), inertially referenced acceleration is obtained simply by adding the gravitational acceleration to the specific force:

$$\mathbf{a}_{ib}^{i} = \mathbf{f}_{ib}^{i} + \boldsymbol{\gamma}_{ib}^{i}\left(\mathbf{r}_{ib}^{i}\right), \tag{5.18}$$

where (2.141) models the gravitational acceleration, $\boldsymbol{\gamma}_{ib}^{i}$, as a function of Cartesian position in an ECI frame. Strictly, the position should be averaged over the interval t to $t + \tau_i$. However, this would require recursive navigation equations, and the gravitational field varies slowly with position, so it is generally sufficient to use[‡] $\mathbf{r}_{ib}^{i}(-)$.

When the reference frame and resolving axes are the same, the time derivative of velocity is simply acceleration, as shown by (2.77). Thus,

$$\dot{\mathbf{v}}_{ib}^{i} = \mathbf{a}_{ib}^{i}. \tag{5.19}$$

When variations in the acceleration over the velocity update interval are not known, as is the case when the velocity integration is iterated at the IMU output rate, the velocity update equation, obtained by integrating (5.19), is simply[‡]

$$\mathbf{v}_{ib}^{i}(+) = \mathbf{v}_{ib}^{i}(-) + \mathbf{a}_{ib}^{i}\tau_{i}. \tag{5.20}$$

[‡] This paragraph, up to this point, is based on material written by the author for QinetiQ, so comprises QinetiQ copyright material.

From (4.9), (5.18), and (5.19), the velocity update in terms of integrated specific force is

$$\mathbf{v}^i_{ib}(+) = \mathbf{v}^i_{ib}(-) + \boldsymbol{\upsilon}^i_{ib} + \boldsymbol{\gamma}^i_{ib}\tau_i. \tag{5.21}$$

5.2.4 Position Update

In the inertial-frame implementation of the navigation equations, the time derivative of the Cartesian position is simply velocity as the reference frame and resolving axes are the same [see (2.68)]. Thus,

$$\dot{\mathbf{r}}^i_{ib} = \mathbf{v}^i_{ib}. \tag{5.22}$$

In the velocity update step where the variation in acceleration is unknown, $\mathbf{v}^i_{ib}$ is typically modeled as a linear function of time over the interval t to $t + \tau_i$. Integrating (5.22) thus leads to the position being modeled as a quadratic function of time. The velocity is known at the start and finish of the update interval, so the position is updated using

$$\begin{aligned}\mathbf{r}^i_{ib}(+) &= \mathbf{r}^i_{ib}(-) + \left(\mathbf{v}^i_{ib}(-) + \mathbf{v}^i_{ib}(+)\right)\frac{\tau_i}{2}\\ &= \mathbf{r}^i_{ib}(-) + \mathbf{v}^i_{ib}(-)\tau_i + \mathbf{a}^i_{ib}\frac{\tau_i^2}{2}\quad,\\ &= \mathbf{r}^i_{ib}(-) + \mathbf{v}^i_{ib}(+)\tau_i - \mathbf{a}^i_{ib}\frac{\tau_i^2}{2}\end{aligned} \tag{5.23}$$

where the three implementations are equally valid.[‡]

5.3 Earth-Frame Navigation Equations

An ECEF frame is commonly used as the reference frame and resolving axes for computation of satellite navigation solutions (Section 9.4), so, in an integrated system, there are benefits in using the same frame for computation of the inertial navigation solution. For some applications, such as airborne photogrammetry, the final navigation solution is more conveniently expressed in an ECEF frame [4]. A disadvantage of an ECEF-frame implementation, compared to an inertial-frame implementation, is that the rotation of the reference frame used for navigation solution computation with respect to an inertial reference, used for the inertial sensor measurements, introduces additional complexity. Figure 5.6 is a block diagram showing how the angular-rate and specific-force measurements are used to update the Earth-referenced attitude, velocity, and position. Each of the four steps is described in turn.

[‡] This paragraph, up to this point, is based on material written by the author for QinetiQ, so comprises QinetiQ copyright material.

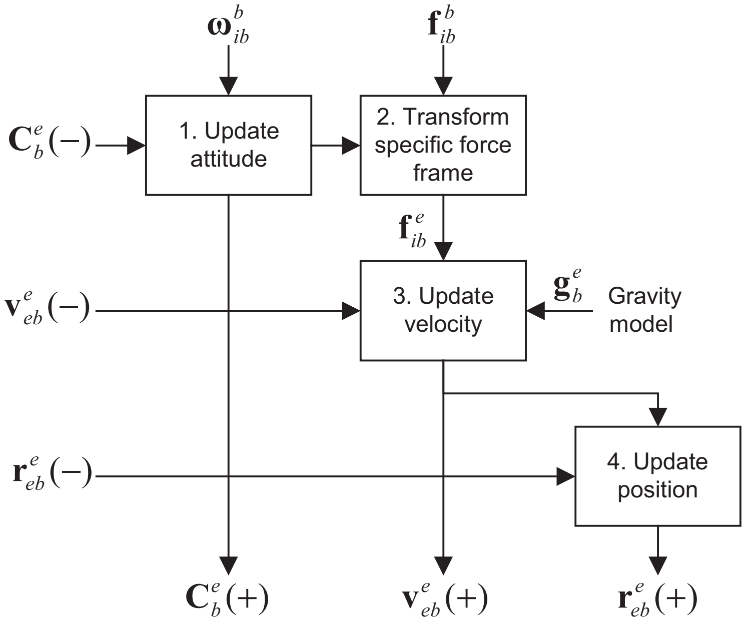

Figure 5.6 Block diagram of ECEF-frame navigation equations.

5.3.1 Attitude Update

The attitude update step of the ECEF-frame navigation equations uses the angular-rate measurement, $\boldsymbol{\omega}_{ib}^{b}$, to update the attitude solution, expressed as the body-to-Earth-frame coordinate transformation matrix, $\mathbf{C}_{b}^{e}$. From (2.56), (2.48), and (2.51), the time derivative is

$$\begin{aligned}\dot{\mathbf{C}}_{b}^{e} &= \mathbf{C}_{b}^{e}\boldsymbol{\Omega}_{eb}^{b} \\ &= \mathbf{C}_{b}^{e}\boldsymbol{\Omega}_{ib}^{b} - \boldsymbol{\Omega}_{ie}^{e}\mathbf{C}_{b}^{e}\end{aligned}, \tag{5.24}$$

where $\boldsymbol{\Omega}_{ib}^{b}$ is the skew-symmetric matrix of the IMU's angular-rate measurement, and $\boldsymbol{\Omega}_{ie}^{e}$ is the skew-symmetric matrix of the Earth-rotation vector. Thus, the rotation of the Earth must be accounted for in updating the attitude. From (2.122),

$$\boldsymbol{\Omega}_{ie}^{e} = \begin{pmatrix} 0 & -\omega_{ie} & 0 \\ \omega_{ie} & 0 & 0 \\ 0 & 0 & 0 \end{pmatrix}. \tag{5.25}$$

Integrating (5.24) gives

$$\begin{aligned}\mathbf{C}_{b}^{e}(t+\tau_i) &\approx \mathbf{C}_{b}^{e}(t)\exp\left(\boldsymbol{\Omega}_{eb}^{b}\tau_i\right) \\ &= \mathbf{C}_{b}^{e}(t)\exp\left[\left(\boldsymbol{\Omega}_{ib}^{b} - \boldsymbol{\Omega}_{ie}^{e}\right)\tau_i\right] \\ &= \mathbf{C}_{b}^{e}(t)\exp\left(\boldsymbol{\Omega}_{ib}^{b}\tau_i\right) - \mathbf{C}_{b}^{e}(t)\left[\exp\left(\boldsymbol{\Omega}_{ie}^{b}\tau_i\right) - \mathbf{I}_3\right] \\ &= \mathbf{C}_{b}^{e}(t)\exp\left(\left[\boldsymbol{\alpha}_{ib}^{b}\wedge\right]\right) - \left[\exp\left(\boldsymbol{\Omega}_{ie}^{e}\tau_i\right) - \mathbf{I}_3\right]\mathbf{C}_{b}^{e}(t)\end{aligned}, \tag{5.26}$$

noting that $\mathbf{\Omega}_{ie}^{e}$ is assumed constant. As in an ECI-frame implementation, the exponents must be computed as power-series expansions. Applying the small angle approximation by truncating the expansions at the first order and assuming the IMU angular-rate measurement is constant over the integration interval (i.e., $\boldsymbol{\alpha}_{ib}^{b} \approx \boldsymbol{\omega}_{ib}^{b}\tau_i$) give

$$\mathbf{C}_b^e(+) \approx \mathbf{C}_b^e(-)\left(\mathbf{I}_3 + \mathbf{\Omega}_{ib}^{b}\tau_i\right) - \mathbf{\Omega}_{ie}^{e}\mathbf{C}_b^e(-)\tau_i. \tag{5.27}$$

As the Earth rotation rate is very slow compared to the angular rates measured by the IMU, this small angle approximation is always valid for the Earth rate term of the attitude update equation. However, as discussed in Sections 5.2.1 and 5.5.1, most applications require a more precise implementation of the gyro measurement term.

5.3.2 Specific-Force Frame Transformation

The specific-force frame transformation takes the same form as in an inertial-frame implementation:

$$\begin{aligned} \mathbf{f}_{ib}^{e}(t) &= \mathbf{C}_b^e(t)\mathbf{f}_{ib}^{b}(t) \\ \Rightarrow \mathbf{f}_{ib}^{e} &\approx \tfrac{1}{2}\left(\mathbf{C}_b^e(-) + \mathbf{C}_b^e(+)\right)\mathbf{f}_{ib}^{b} \end{aligned}. \tag{5.28}$$

or

$$\begin{aligned} \boldsymbol{\upsilon}_{ib}^{e} &= \bar{\mathbf{C}}_b^e\boldsymbol{\upsilon}_{ib}^{b} \\ &\approx \tfrac{1}{2}\left(\mathbf{C}_b^e(-) + \mathbf{C}_b^e(+)\right)\boldsymbol{\upsilon}_{ib}^{b} \end{aligned}. \tag{5.29}$$

5.3.3 Velocity Update

As in an inertial-frame implementation, the reference frame and resolving axes are the same so, from (2.76) and (2.77),

$$\dot{\mathbf{v}}_{eb}^{e} = \mathbf{a}_{eb}^{e} = \ddot{\mathbf{r}}_{eb}^{e}. \tag{5.30}$$

Now, applying (2.61), (2.65), and (2.66) in turn,

$$\begin{aligned} \mathbf{r}_{eb}^{e} &= \mathbf{r}_{ib}^{e} - \mathbf{r}_{ie}^{e} \\ &= \mathbf{r}_{ib}^{e} \end{aligned}. \tag{5.31}$$

Substituting this into (5.30),

$$\dot{\mathbf{v}}_{eb}^{e} = \ddot{\mathbf{r}}_{ib}^{e}. \tag{5.32}$$

Applying (2.81), noting that the Earth rate, $\boldsymbol{\omega}_{ie}^{e}$, is constant,

$$\dot{\mathbf{v}}_{eb}^{e} = -\boldsymbol{\Omega}_{ie}^{e}\boldsymbol{\Omega}_{ie}^{e}\mathbf{r}_{ib}^{e} - 2\boldsymbol{\Omega}_{ie}^{e}\dot{\mathbf{r}}_{eb}^{e} + \mathbf{a}_{ib}^{e}. \tag{5.33}$$

Thus, the rate of change of velocity resolved about the Earth-frame axes incorporates a centrifugal and a Coriolis term due to the rotation of the resolving axes as explained in Section 2.3.5. Applying (2.66) and (2.67),

$$\dot{\mathbf{v}}_{eb}^{e} = -\boldsymbol{\Omega}_{ie}^{e}\boldsymbol{\Omega}_{ie}^{e}\mathbf{r}_{eb}^{e} - 2\boldsymbol{\Omega}_{ie}^{e}\mathbf{v}_{eb}^{e} + \mathbf{a}_{ib}^{e}. \tag{5.34}$$

From (2.125), the applied acceleration, $\mathbf{a}_{ib}^{e}$, is the sum of the measured specific force, $\mathbf{f}_{ib}^{e}$, and the acceleration due to the gravitational force, $\boldsymbol{\gamma}_{ib}^{e}$. From (2.132), the acceleration due to gravity, $\mathbf{g}_{b}^{e}$, is the sum of the gravitational and centrifugal accelerations. Substituting these into (5.34),

$$\dot{\mathbf{v}}_{eb}^{e} = \mathbf{f}_{ib}^{e} + \mathbf{g}_{b}^{e}\left(\mathbf{r}_{eb}^{e}\right) - 2\boldsymbol{\Omega}_{ie}^{e}\mathbf{v}_{eb}^{e}. \tag{5.35}$$

An analytical solution is complex. However, as the Coriolis term will be much smaller than the specific-force and gravity terms, except for space applications, it is a reasonable approximation to neglect the variation of the Coriolis term over the integration interval. Thus,

$$\begin{aligned}\mathbf{v}_{eb}^{e}(+) &\approx \mathbf{v}_{eb}^{e}(-) + \left(\mathbf{f}_{ib}^{e} + \mathbf{g}_{b}^{e}\left(\mathbf{r}_{eb}^{e}(-)\right) - 2\boldsymbol{\Omega}_{ie}^{e}\mathbf{v}_{eb}^{e}(-)\right)\tau_i \\ &= \mathbf{v}_{eb}^{e}(-) + \boldsymbol{\upsilon}_{ib}^{e} + \left(\mathbf{g}_{b}^{e}\left(\mathbf{r}_{eb}^{e}(-)\right) - 2\boldsymbol{\Omega}_{ie}^{e}\mathbf{v}_{eb}^{e}(-)\right)\tau_i\end{aligned}. \tag{5.36}$$

Most gravity models operate as a function of latitude and height, calculated from Cartesian ECEF position using (2.113). The gravity is converted from local navigation frame to ECEF resolving axes by premultiplying by $\mathbf{C}_{n}^{e}$, given by (2.150). Alternatively, a gravity model formulated in ECEF axes is presented in [4].

5.3.4 Position Update

In ECEF-frame navigation equations, the reference and resolving frames are the same, so, from (2.68),

$$\dot{\mathbf{r}}_{eb}^{e} = \mathbf{v}_{eb}^{e}. \tag{5.37}$$

Integrating this, assuming the velocity varies linearly over the integration interval,

$$\begin{aligned}\mathbf{r}_{eb}^{e}(+) &= \mathbf{r}_{eb}^{e}(-) + \left(\mathbf{v}_{eb}^{e}(-) + \mathbf{v}_{eb}^{e}(+)\right)\frac{\tau_i}{2} \\ &\approx \mathbf{r}_{eb}^{e}(-) + \mathbf{v}_{eb}^{e}(-)\tau_i + \left(\mathbf{f}_{ib}^{e} + \mathbf{g}_{b}^{e}\left(\mathbf{r}_{eb}^{e}(-)\right) - 2\boldsymbol{\Omega}_{ie}^{e}\mathbf{v}_{eb}^{e}(-)\right)\frac{\tau_i^2}{2}\end{aligned}. \tag{5.38}$$

5.4 Local-Navigation-Frame Navigation Equations

In a local-navigation-frame implementation of the inertial navigation equations, an ECEF frame is used as the reference frame while a local navigation frame (north, east, down) comprises the resolving axes. Thus, attitude is expressed as the body-to-navigation-frame coordinate transformation matrix, $\mathbf{C}_b^n$, and velocity is Earth-referenced in local navigation frame axes, $\mathbf{v}_{eb}^n$. Position is expressed in the curvilinear form (i.e., as geodetic latitude, L_b, longitude, λ_b, and geodetic height, h_b) and is commonly integrated directly from the velocity rather than converted from its Cartesian form.

This form of navigation equations has the advantage of providing a navigation solution in a form readily suited for user output. However, additional complexity is introduced, compared to ECI- and ECEF-frame implementations, as the orientation of the resolving axes with respect to the reference frame depends on the position. Figure 5.7 is a block diagram showing how the angular-rate and specific-force measurements are used to update the attitude, velocity, and position in a local-navigation-frame implementation. Each of the four steps is described in turn. This is followed by a brief discussion of the related wander-azimuth implementation.

5.4.1 Attitude Update

The attitude update step of the local-navigation-frame navigation equations uses the position and velocity solution as well as the angular-rate measurement to update $\mathbf{C}_b^n$. This is necessary because the orientation of the north, east, and down axes changes as the navigation system moves with respect to the Earth, as explained in Section 2.1.3. From (2.56), the time derivative of the coordinate transformation matrix is

$$\dot{\mathbf{C}}_b^n = \mathbf{C}_b^n \mathbf{\Omega}_{nb}^b. \qquad (5.39)$$

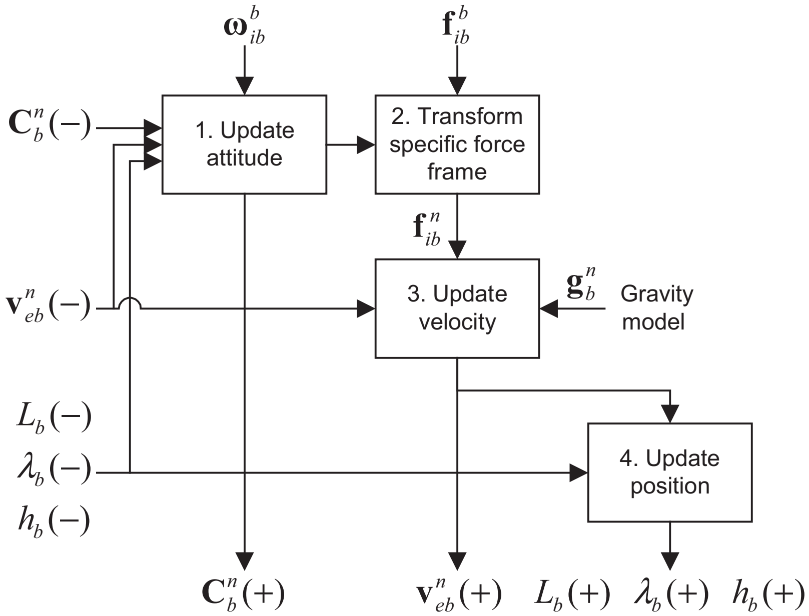

Figure 5.7 Block diagram of local-navigation-frame navigation equations.

Using (2.48) and (2.51), this may be split into three terms:

$$\dot{\mathbf{C}}_b^n = \mathbf{C}_b^n \boldsymbol{\Omega}_{ib}^b - \left(\boldsymbol{\Omega}_{ie}^n + \boldsymbol{\Omega}_{en}^n\right)\mathbf{C}_b^n. \tag{5.40}$$

The first term is due to the inertially referenced angular rate, measured by the gyros, and the second is due to the rotation of the Earth with respect to an inertial frame. The third term, known as the *transport rate*, arises from the rotation of the local-navigation-frame axes as the frame center (i.e., the navigation system) moves with respect to the Earth. When the attitude of the body frame with respect to the local navigation frame remains constant, the gyros sense the Earth rotation and transport rate, which must be corrected for to keep the attitude unchanged.

The Earth-rotation vector in local navigation frame axes is given by (2.123), so the skew-symmetric matrix is

$$\boldsymbol{\Omega}_{ie}^n = \omega_{ie}\begin{pmatrix} 0 & \sin L_b & 0 \\ -\sin L_b & 0 & -\cos L_b \\ 0 & \cos L_b & 0 \end{pmatrix}, \tag{5.41}$$

noting that this is a function of latitude.
From (2.56), the transport rate may be obtained by solving

$$\dot{\mathbf{C}}_e^n = -\boldsymbol{\Omega}_{en}^n \mathbf{C}_e^n. \tag{5.42}$$

The ECEF-to-local-navigation-frame coordinate transformation matrix is given by (2.150). Taking the time derivative of this gives

$$\dot{\mathbf{C}}_e^n = \left[\begin{pmatrix} -\dot{\lambda}_b \cos L_b \\ \dot{L}_b \\ \dot{\lambda}_b \sin L_b \end{pmatrix} \wedge \right]\mathbf{C}_e^n. \tag{5.43}$$

Substituting this into (5.42), together with the derivatives of the latitude and longitude from (2.111) gives

$$\begin{gathered} \boldsymbol{\Omega}_{en}^n = \begin{pmatrix} 0 & -\omega_{en,z}^n & \omega_{en,y}^n \\ \omega_{en,z}^n & 0 & -\omega_{en,x}^n \\ -\omega_{en,y}^n & \omega_{en,x}^n & 0 \end{pmatrix} \\ \boldsymbol{\omega}_{en}^n = \begin{pmatrix} v_{eb,E}^n \big/ \left(R_E(L_b) + h_b\right) \\ -v_{eb,N}^n \big/ \left(R_N(L_b) + h_b\right) \\ -v_{eb,E}^n \tan L_b \big/ \left(R_E(L_b) + h_b\right) \end{pmatrix} \end{gathered}. \tag{5.44}$$

Integrating (5.39) gives

$$\begin{aligned}\mathbf{C}_b^n(t+\tau_i) &\approx \mathbf{C}_b^n(t)\exp\left(\boldsymbol{\Omega}_{nb}^b\tau_i\right)\\ &= \mathbf{C}_b^n(t)\exp\left[\left(\boldsymbol{\Omega}_{ib}^b-\boldsymbol{\Omega}_{ie}^b-\boldsymbol{\Omega}_{en}^b\right)\tau_i\right]\\ &= \mathbf{C}_b^n(t)\exp\left(\boldsymbol{\Omega}_{ib}^b\tau_i\right)-\mathbf{C}_b^n(t)\left\{\exp\left[\left(\boldsymbol{\Omega}_{ie}^b+\boldsymbol{\Omega}_{en}^b\right)\tau_i\right]-\mathbf{I}_3\right\}\\ &= \mathbf{C}_b^n(t)\exp\left(\left[\boldsymbol{\alpha}_{ib}^b\wedge\right]\right)-\left\{\exp\left[\left(\boldsymbol{\Omega}_{ie}^n+\boldsymbol{\Omega}_{en}^n\right)\tau_i\right]-\mathbf{I}_3\right\}\mathbf{C}_b^n(t)\end{aligned}, \quad (5.45)$$

where the position and velocity, and hence $\boldsymbol{\Omega}_{ie}^n$ and $\boldsymbol{\Omega}_{en}^n$, are assumed constant over the attitude update interval. Accounting for their variation can require recursive navigation equations as discussed in Section 5.5. However, a reasonable approximation to (5.45) for most applications can be obtained by neglecting the position and velocity variation and truncating the power-series expansion of the Earth-rotation and transport rate terms to first order. Applying the first-order approximation to all terms gives

$$\mathbf{C}_b^n(+)\approx\mathbf{C}_b^n(-)\left(\mathbf{I}_3+\boldsymbol{\Omega}_{ib}^b\tau_i\right)-\left(\boldsymbol{\Omega}_{ie}^n(-)+\boldsymbol{\Omega}_{en}^n(-)\right)\mathbf{C}_b^n(-)\tau_i, \quad (5.46)$$

where $\boldsymbol{\Omega}_{ie}^n(-)$ is calculated using $L_b(-)$ and $\boldsymbol{\Omega}_{en}^n(-)$ is calculated using $L_b(-)$, $h_b(-)$, and $\mathbf{v}_{eb}^n(-)$. As discussed in Section 5.2.1, a more precise implementation of the gyro measurement term is required for most applications. Higher precision solutions are discussed in Section 5.5.1.

5.4.2 Specific-Force Frame Transformation

The specific-force frame transformation is essentially the same as for the ECI and ECEF-frame implementations. Thus,

$$\begin{aligned}\mathbf{f}_{ib}^n(t) &= \mathbf{C}_b^n(t)\mathbf{f}_{ib}^b(t)\\ \Rightarrow \mathbf{f}_{ib}^n &\approx \tfrac{1}{2}\left(\mathbf{C}_b^n(-)+\mathbf{C}_b^n(+)\right)\mathbf{f}_{ib}^b\end{aligned}, \quad (5.47)$$

or

$$\begin{aligned}\boldsymbol{\upsilon}_{ib}^n &= \bar{\mathbf{C}}_b^n\boldsymbol{\upsilon}_{ib}^b\\ &\approx \tfrac{1}{2}\left(\mathbf{C}_b^n(-)+\mathbf{C}_b^n(+)\right)\boldsymbol{\upsilon}_{ib}^b\end{aligned}. \quad (5.48)$$

The accuracy of this approximation will be similar to that in an inertial frame as the gyro-sensed rotation will usually be much larger than the Earth rate and transport rate components.[‡]

[‡] This paragraph, up to this point, is based on material written by the author for QinetiQ, so comprises QinetiQ copyright material.

5.4.3 Velocity Update

In the local-navigation-frame navigation equations, the resolving axes of the velocity are not the same as its reference frame. From (2.73), the velocity is expressed in terms in terms of its counterpart in ECEF resolving axes by

$$\mathbf{v}_{eb}^{n} = \mathbf{C}_{e}^{n}\mathbf{v}_{eb}^{e}. \tag{5.49}$$

Differentiating this,

$$\dot{\mathbf{v}}_{eb}^{n} = \dot{\mathbf{C}}_{e}^{n}\mathbf{v}_{eb}^{e} + \mathbf{C}_{e}^{n}\dot{\mathbf{v}}_{eb}^{e}. \tag{5.50}$$

Thus, there is a transport-rate term in addition to the applied acceleration, centrifugal, and Coriolis terms found in the ECEF-frame velocity update described in Section 5.3.3. Applying (2.56) and (2.73) to the first term and substituting (5.34) for the second term,

$$\dot{\mathbf{v}}_{eb}^{n} = -\boldsymbol{\Omega}_{en}^{n}\mathbf{v}_{eb}^{n} + \mathbf{C}_{e}^{n}\left(-\boldsymbol{\Omega}_{ie}^{e}\boldsymbol{\Omega}_{ie}^{e}\mathbf{r}_{eb}^{e} - 2\boldsymbol{\Omega}_{ie}^{e}\mathbf{v}_{eb}^{e} + \mathbf{a}_{ib}^{e}\right). \tag{5.51}$$

Applying (2.51), (2.62), (2.73), and (2.83) to transform the resolving axes and rearranging give

$$\dot{\mathbf{v}}_{eb}^{n} = -\boldsymbol{\Omega}_{ie}^{n}\boldsymbol{\Omega}_{ie}^{n}\mathbf{r}_{eb}^{n} - \left(\boldsymbol{\Omega}_{en}^{n} + 2\boldsymbol{\Omega}_{ie}^{n}\right)\mathbf{v}_{eb}^{n} + \mathbf{a}_{ib}^{n}, \tag{5.52}$$

noting that the skew-symmetric matrices of the Earth rotation and transport rate are given by (5.41) and (5.44), respectively.

Expressing the acceleration in terms of the specific force, gravity, and centrifugal acceleration using (2.125) and (2.132) gives

$$\dot{\mathbf{v}}_{eb}^{n} = \mathbf{f}_{ib}^{n} + \mathbf{g}_{b}^{n}\left(L_{b}, h_{b}\right) - \left(\boldsymbol{\Omega}_{en}^{n} + 2\boldsymbol{\Omega}_{ie}^{n}\right)\mathbf{v}_{eb}^{n}, \tag{5.53}$$

where the acceleration due to gravity is modeled as a function of latitude and height. Again, obtaining a full analytical solution is complex. However, as the Coriolis and transport-rate terms will generally be the smallest, it is a reasonable approximation to neglect their variation over the integration interval. Again, the variation of the acceleration due to gravity over the integration interval can generally be neglected. Thus,

$$\begin{aligned} \mathbf{v}_{eb}^{n}(+) &\approx \mathbf{v}_{eb}^{n}(-) + \left[\mathbf{f}_{ib}^{n} + \mathbf{g}_{b}^{n}\left(L_{b}(-), h_{b}(-)\right) - \left(\boldsymbol{\Omega}_{en}^{n}(-) + 2\boldsymbol{\Omega}_{ie}^{n}(-)\right)\mathbf{v}_{eb}^{n}(-)\right]\tau_{i} \\ &= \mathbf{v}_{eb}^{n}(-) + \boldsymbol{\upsilon}_{ib}^{n} + \left[\mathbf{g}_{b}^{n}\left(L_{b}(-), h_{b}(-)\right) - \left(\boldsymbol{\Omega}_{en}^{n}(-) + 2\boldsymbol{\Omega}_{ie}^{n}(-)\right)\mathbf{v}_{eb}^{n}(-)\right]\tau_{i} \end{aligned}. \tag{5.54}$$

5.4.4 Position Update

From (2.111), the derivatives of the latitude, longitude, and height are functions of the velocity, latitude, and height. Thus,*

*This and subsequent paragraphs are based on material written by the author for QinetiQ, so comprise QinetiQ copyright material.

$$
\begin{aligned}
L_b(+) &= L_b(-) + \int_t^{t+\tau_i} \frac{v_{eb,N}^n(t')}{R_N(L_b(t')) + h_b(t')}\,dt' \\
\lambda_b(+) &= \lambda_b(-) + \int_t^{t+\tau_i} \frac{v_{eb,E}^n(t')}{\big(R_E(L_b(t')) + h_b(t')\big)\cos L_b(t')}\,dt'. \\
h_b(+) &= h_b(-) - \int_t^{t+\tau_i} v_{eb,D}^n(t')\,dt'
\end{aligned}
\qquad (5.55)
$$

The variation of the meridian and transverse radii of curvature, R_N and R_E, with the geodetic latitude, L_b, is weak, so it is acceptable to neglect their variation with latitude over the integration interval. Assuming the velocity varies as a linear function of time over the integration interval, a suitable approximation for the position update is

$$
\begin{aligned}
h_b(+) &= h_b(-) - \frac{\tau_i}{2}\left(v_{eb,D}^n(-) + v_{eb,D}^n(+)\right) \\
L_b(+) &\approx L_b(-) + \frac{\tau_i}{2}\left(\frac{v_{eb,N}^n(-)}{R_N(L_b(-)) + h_b(-)} + \frac{v_{eb,N}^n(+)}{R_N(L_b(-)) + h_b(+)}\right) \\
\lambda_b(+) &= \lambda_b(-) + \frac{\tau_i}{2}\left(\frac{v_{eb,E}^n(-)}{\big(R_E(L_b(-)) + h_b(-)\big)\cos L_b(-)} + \frac{v_{eb,E}^n(+)}{\big(R_E(L_b(+)) + h_b(+)\big)\cos L_b(+)}\right)
\end{aligned}
\quad , \qquad (5.56)
$$

noting that the height, latitude, and longitude should be calculated in that order.† The longitude update does not work at the poles because $1/\cos L_b$ approaches infinity.

Alternatively, the position may be updated by solving

$$
\dot{\mathbf{C}}_n^e = \mathbf{C}_n^e \boldsymbol{\Omega}_{en}^n, \qquad (5.57)
$$

where (2.150) and (2.151) provide the conversion between $\mathbf{C}_n^e$ and L_b and λ_b. A first-order solution is

$$
\mathbf{C}_n^e(+) \approx \mathbf{C}_n^e(-)\Big(\mathbf{I}_3 + \tfrac{1}{2}\big(\boldsymbol{\Omega}_{en}^n(-) + \boldsymbol{\Omega}_{en}^n(+)\big)\tau_i\Big), \qquad (5.58)
$$

where $\boldsymbol{\Omega}_{en}^n(-)$ and $\boldsymbol{\Omega}_{en}^n(+)$ are computed using (5.44) from $\mathbf{v}_{eb}^n(-)$ and $\mathbf{v}_{eb}^n(+)$, respectively. This approach also fails at the poles because $\omega_{en,z}^e$ approaches infinity.

5.4.5 Wander-Azimuth Implementation

Inertial navigation equations can be mechanized in the axes of a wander-azimuth frame to minimize the effects of the polar singularities that occur in a local navigation frame [5]. A wander-azimuth coordinate frame (see Section 2.1.6), denoted by w, is closely related to the corresponding local navigation frame. The z-axis is

†End of QinetiQ copyright material.

coincidental, pointing down, but the x- and y-axes are rotated about the z-axis with respect to the local navigation frame by a wander angle that varies with position. The wander angle is simply the heading (or azimuthal) Euler angle from the local navigation frame to the wander azimuth frame, ψ_{nw}, although many authors use α. Thus, from (2.22) and (2.24),

$$\mathbf{C}_n^w = \begin{pmatrix} \cos\psi_{nw} & \sin\psi_{nw} & 0 \\ -\sin\psi_{nw} & \cos\psi_{nw} & 0 \\ 0 & 0 & 1 \end{pmatrix} \qquad \mathbf{C}_w^n = \begin{pmatrix} \cos\psi_{nw} & -\sin\psi_{nw} & 0 \\ \sin\psi_{nw} & \cos\psi_{nw} & 0 \\ 0 & 0 & 1 \end{pmatrix}. \tag{5.59}$$

The wander angle is generally initialized at zero at the start of navigation. Note that some authors use the wander angle with the opposing sign, ψ_{wn}, which may also be denoted as α.

Latitude and longitude in a wander-azimuth implementation are replaced by the ECEF frame to wander-azimuth frame coordinate transformation matrix, $\mathbf{C}_e^w$. From (2.15), (2.150), and (5.59), this may expressed in terms of the latitude, longitude, and wander angle using

$$\mathbf{C}_e^w = \begin{bmatrix} \begin{pmatrix} -\sin L_b \cos\lambda_b \cos\psi_{nw} \\ -\sin\lambda_b \sin\psi_{nw} \end{pmatrix} & \begin{pmatrix} -\sin L_b \sin\lambda_b \cos\psi_{nw} \\ +\cos\lambda_b \sin\psi_{nw} \end{pmatrix} & \cos L_b \cos\psi_{nw} \\ \begin{pmatrix} \sin L_b \cos\lambda_b \sin\psi_{nw} \\ -\sin\lambda_b \cos\psi_{nw} \end{pmatrix} & \begin{matrix} \sin L_b \sin\lambda_b \sin\psi_{nw} \\ +\cos\lambda_b \cos\psi_{nw} \end{matrix} & -\cos L_b \sin\psi_{nw} \\ -\cos L_b \cos\lambda_b & -\cos L_b \sin\lambda_b & -\sin L_b \end{bmatrix}. \tag{5.60}$$

Conversely,

$$\begin{aligned} L_b &= -\arcsin\left(C_{e,3,3}^w\right) \\ \lambda_b &= \arctan_2\left(-C_{e,3,2}^w, -C_{e,3,1}^w\right), \\ \psi_{nw} &= \arctan_2\left(-C_{e,2,3}^w, C_{e,1,3}^w\right) \end{aligned} \tag{5.61}$$

noting that the longitude and wander angle are undefined at the poles ($L_b = \pm 90°$) and may be subject to significant computational rounding errors near the poles.

The attitude, velocity, and height inertial navigation equations in a wander-azimuth frame are as those for a local navigation frame, presented earlier, with w substituted for n, except that the transport-rate term has no component about the vertical axis. Thus,

$$\boldsymbol{\omega}_{ew}^w = \mathbf{C}_n^w \begin{pmatrix} \omega_{en,N}^n \\ \omega_{en,E}^n \\ 0 \end{pmatrix}. \tag{5.62}$$

From (5.44), this may be obtained from the wander-azimuth-resolved velocity using

$$
\begin{aligned}
\boldsymbol{\omega}_{ew}^{w} &= \mathbf{C}_{n}^{w}\begin{pmatrix} 0 & 1\Big/\left(R_E(C_{e,3,3}^{w})+h_b\right) & 0 \\ -1\Big/\left(R_N(C_{e,3,3}^{w})+h_b\right) & 0 & 0 \\ 0 & 0 & 0 \end{pmatrix}\mathbf{C}_{w}^{n}\mathbf{v}_{eb}^{w} \\
&= \begin{pmatrix} \dfrac{\cos\psi_{nw}\sin\psi_{nw}}{R_E(C_{e,3,3}^{w})+h_b}-\dfrac{\cos\psi_{nw}\sin\psi_{nw}}{R_N(C_{e,3,3}^{w})+h_b} & \dfrac{\cos^2\psi_{nw}}{R_E(C_{e,3,3}^{w})+h_b}+\dfrac{\sin^2\psi_{nw}}{R_N(C_{e,3,3}^{w})+h_b} & 0 \\ -\dfrac{\cos^2\psi_{nw}}{R_N(C_{e,3,3}^{w})+h_b}-\dfrac{\sin^2\psi_{nw}}{R_E(C_{e,3,3}^{w})+h_b} & \dfrac{\cos\psi_{nw}\sin\psi_{nw}}{R_N(C_{e,3,3}^{w})+h_b}-\dfrac{\cos\psi_{nw}\sin\psi_{nw}}{R_E(C_{e,3,3}^{w})+h_b} & 0 \\ 0 & 0 & 0 \end{pmatrix}\mathbf{v}_{eb}^{w}
\end{aligned}
\qquad (5.63)
$$

where from (2.105), (2.106), and (5.61), the meridian and transverse radii of curvature may be expressed directly in terms of $C_{e,3,3}^{w}$ using

$$
R_N(C_{e,3,3}^{w}) = \frac{R_0\left(1-e^2\right)}{\left(1-e^2 C_{e,3,3}^{w\;2}\right)^{3/2}}, \qquad R_E(C_{e,3,3}^{w}) = \frac{R_0}{\sqrt{1-e^2 C_{e,3,3}^{w\;2}}}. \qquad (5.64)
$$

At the poles, $R_N = R_E = R_0\big/\sqrt{1-e^2}$. Therefore, near the poles (e.g., where $\left|C_{e,3,3}^{w}\right| > 0.99995$), (5.63) may be replaced by

$$
\boldsymbol{\omega}_{ew}^{w} \approx \frac{1}{\dfrac{R_0}{\sqrt{1-e^2}}+h_b}\begin{pmatrix} 0 & 1 & 0 \\ -1 & 0 & 0 \\ 0 & 0 & 0 \end{pmatrix}\mathbf{v}_{eb}^{w}, \qquad (5.65)
$$

avoiding the need to compute the wander angle.

The Earth-rotation vector is, from (2.143),

$$
\boldsymbol{\omega}_{ie}^{w} = \mathbf{C}_{n}^{w}\boldsymbol{\omega}_{ie}^{n}. \qquad (5.66)
$$

To the first order in time, the latitude and longitude may be updated using

$$
\mathbf{C}_{e}^{w}(+) \approx \left(\mathbf{I}_3 - \tfrac{1}{2}\left(\boldsymbol{\Omega}_{ew}^{w}(-)+\boldsymbol{\Omega}_{ew}^{w}(+)\right)\tau_i\right)\mathbf{C}_{e}^{w}(-), \qquad (5.67)
$$

where $\boldsymbol{\Omega}_{ew}^{w}(-)$ and $\boldsymbol{\Omega}_{ew}^{w}(+)$ are computed using (5.63) from $\mathbf{v}_{eb}^{w}(-)$ and $\mathbf{v}_{eb}^{w}(+)$, respectively.

The height may be updated using (5.56), noting that $v_{eb,D}^{n} = v_{eb,z}^{w}$.

5.5 Navigation Equations Optimization

The inertial navigation equations presented in the preceding sections are approximate and exhibit errors that increase with the host vehicle dynamics, vibration level, and update interval. This section presents precision navigation equations that offer higher accuracy at the cost of greater complexity and processing load. This is followed by a discussion of the effects of the sensor sampling interval and vibration, including coning and sculling errors, and their mitigation. The section concludes with a discussion of the design tradeoffs that must be made in selecting suitable iteration rates and approximations for different inertial navigation applications. Factors to consider include performance requirements, operating environment, sensor quality, processing capacity, and available development time.

The MATLAB functions on the CD, Nav_equations_ECI, Nav_equations_ECEF, and Nav_equations_NED, respectively, implement the ECI-frame, ECEF-frame, and local-navigation-frame versions of the precision inertial navigation equations described in this section.

5.5.1 Precision Attitude Update

It is convenient to define the attitude update matrix as the coordinate transformation matrix from the body frame at the end of the attitude update step of the navigation equations to that at the beginning, $\mathbf{C}_{b+}^{b-}$ (some authors use $\mathbf{A}$). It may be used to define the attitude update step in an ECI frame; thus,

$$\begin{aligned}\mathbf{C}_b^i(+) &= \mathbf{C}_b^i(-)\mathbf{C}_{b+}^{b-}\\ \mathbf{C}_{b+}^{b-} &= \mathbf{C}_i^b(-)\mathbf{C}_b^i(+)\end{aligned}\ . \tag{5.68}$$

Substituting (5.10) and (5.11) into (5.68) defines the attitude update matrix in terms of the attitude increment, $\boldsymbol{\alpha}_{ib}^b$:

$$\mathbf{C}_{b+}^{b-} = \mathbf{C}_{b(t+\tau_i)}^{b(t)} = \exp\left[\boldsymbol{\alpha}_{ib}^b\ \wedge\right] = \sum_{r=0}^{\infty}\frac{\left[\boldsymbol{\alpha}_{ib}^b\ \wedge\right]^r}{r!} \tag{5.69}$$

where a constant angular rate is assumed.

When the power-series expansion is truncated, errors arise depending on the step size of the attitude increment and the order at which the power series is truncated. Table 5.1 presents some examples [1]. Clearly, the third- and fourth-order algorithms perform significantly better than the first- and second-order algorithms. It should also be noted that the error varies as the square of the attitude increment for the first- and second-order algorithms, but as the fourth power for the third- and fourth-order variants. Thus, with the higher-order algorithms, increasing the iteration rate has more impact on the accuracy.

In practice, there are few applications where the host vehicle rotates continuously in the same direction, while errors arising from angular oscillation about

Table 5.1 Drift of First- to Fourth-Order Attitude Update Algorithms at an Update Rate of 100 Hz

Algorithm Order	*Attitude Drift at 100-Hz update rate, rad s^{-1} (° hr^{-1})*	
	$\lvert\alpha\rvert = 0.1$ rad step size	$\lvert\alpha\rvert = 0.05$ rad step size
1	0.033 (6,830)	8.3×10^{-3} (1,720)
2	0.017 (3,430)	4.2×10^{-3} (860)
3	3.4×10^{-5} (6.9)	2.5×10^{-6} (0.4)
4	8.3×10^{-6} (1.7)	5.2×10^{-7} (0.1)

a single axis cancel out over time. Problems generally occur when there is synchronized angular oscillation about two axes, known as coning, in which case using the first-order attitude update leads to an attitude drift about the mutually perpendicular axis that is generally proportional to the product of the amplitudes of the two oscillations and does not change sign. Thus, the ensuing attitude error increases with time. Similar errors occur in the presence of synchronized angular and linear oscillation, known as sculling. Coning and sculling are discussed further in Section 5.5.4.

The third and fourth powers of a skew-symmetric matrix have the following properties:

$$\begin{aligned}\left[\mathbf{x}\wedge\right]^3 &= -\lvert\mathbf{x}\rvert^2\left[\mathbf{x}\wedge\right] \\ \left[\mathbf{x}\wedge\right]^4 &= -\lvert\mathbf{x}\rvert^2\left[\mathbf{x}\wedge\right]^2\end{aligned}. \tag{5.70}$$

Substituting this into (5.69):

$$\mathbf{C}_{b+}^{b-} = \mathbf{I}_3 + \left(\sum_{r=0}^{\infty}(-1)^r\frac{\lvert\boldsymbol{\alpha}_{ib}^b\rvert^{2r}}{(2r+1)!}\right)\left[\boldsymbol{\alpha}_{ib}^b\wedge\right] + \left(\sum_{r=0}^{\infty}(-1)^r\frac{\lvert\boldsymbol{\alpha}_{ib}^b\rvert^{2r}}{(2r+2)!}\right)\left[\boldsymbol{\alpha}_{ib}^b\wedge\right]^2. \tag{5.71}$$

The fourth-order approximation is then

$$\mathbf{C}_{b+}^{b-} \approx \mathbf{I}_3 + \left(1-\frac{\lvert\boldsymbol{\alpha}_{ib}^b\rvert^2}{6}\right)\left[\boldsymbol{\alpha}_{ib}^b\wedge\right] + \left(\frac{1}{2}-\frac{\lvert\boldsymbol{\alpha}_{ib}^b\rvert^2}{24}\right)\left[\boldsymbol{\alpha}_{ib}^b\wedge\right]^2. \tag{5.72}$$

However, the power-series expansions in (5.71) are closely related to those of the sine and cosine, so

$$\mathbf{C}_{b+}^{b-} = \mathbf{I}_3 + \frac{\sin\lvert\boldsymbol{\alpha}_{ib}^b\rvert}{\lvert\boldsymbol{\alpha}_{ib}^b\rvert}\left[\boldsymbol{\alpha}_{ib}^b\wedge\right] + \frac{1-\cos\lvert\boldsymbol{\alpha}_{ib}^b\rvert}{\lvert\boldsymbol{\alpha}_{ib}^b\rvert^2}\left[\boldsymbol{\alpha}_{ib}^b\wedge\right]^2. \tag{5.73}$$

This is known as Rodrigues' formula. To avoid division by zero, this should be replaced with the approximate version whenever $\lvert\boldsymbol{\alpha}_{ib}^b\rvert$ is very small.

The ECI-frame attitude update may thus be performed exactly. Note that the inverse of (5.73) gives the attitude increment vector in terms of the attitude update matrix:

$$\boldsymbol{\alpha}_{ib}^{b} = \frac{\mu_{b+b-}}{2\sin\mu_{b+b-}}\begin{pmatrix} C_{b+3,2}^{b-} - C_{b+2,3}^{b-} \\ C_{b+1,3}^{b-} - C_{b+3,1}^{b-} \\ C_{b+2,1}^{b-} - C_{b+1,2}^{b-} \end{pmatrix}, \qquad \mu_{b+b-} = \arccos\left[\frac{\mathrm{Tr}\left(\mathbf{C}_{b+}^{b-}\right) - 1}{2}\right]. \qquad (5.74)$$

A similar approach may be taken with the ECEF-frame attitude update. For precision, the first-order solution, (5.27), is replaced by

$$\begin{aligned} \mathbf{C}_{b}^{e}(+) &= \begin{pmatrix} \cos\omega_{ie}\tau_i & \sin\omega_{ie}\tau_i & 0 \\ -\sin\omega_{ie}\tau_i & \cos\omega_{ie}\tau_i & 0 \\ 0 & 0 & 1 \end{pmatrix}\mathbf{C}_{b}^{e}(-)\mathbf{C}_{b+}^{b-}, \\ &\approx \mathbf{C}_{b}^{e}(-)\mathbf{C}_{b+}^{b-} - \mathbf{\Omega}_{ie}^{e}\mathbf{C}_{b}^{e}(-)\tau_i \end{aligned} \qquad (5.75)$$

where the attitude update matrix is given by (5.73) as before. Note that where the first-order approximation is retained for the Earth-rate term, it introduces an error of only 1.3×10^{-15} rad s^{-1} (7.4×10^{-14} ° hr^{-1}) at a 10-Hz update rate and 1.3×10^{-17} rad s^{-1} (7.4×10^{-16} ° hr^{-1}) at a 100-Hz update rate, which is much less that the bias of even the most accurate gyros. Thus, this is an exact solution for all practical purposes.

In the local-navigation-frame attitude update, there is also a transport-rate term, $\boldsymbol{\omega}_{en}^{n}$, given by (5.44). For velocities up to 467 m s^{-1} (Mach 1.4), this is less than the Earth-rotation rate, so for the vast majority of applications, it is valid to truncate the power-series expansion of $\exp(\mathbf{\Omega}_{en}^{n}\tau)$ to first order. Thus, for improved precision, the first-order solution, (5.46), is replaced by

$$\mathbf{C}_{b}^{n}(+) \approx \mathbf{C}_{b}^{n}(-)\mathbf{C}_{b+}^{b-} - \left(\mathbf{\Omega}_{ie}^{e}(-) + \mathbf{\Omega}_{en}^{n}(-)\right)\mathbf{C}_{b}^{n}(-)\tau_i. \qquad (5.76)$$

However, for high-precision, high-dynamic applications, the variation of the transport rate over the update interval can be significant. When a high-precision specific-force frame transformation (Section 5.5.2) is implemented, the updated attitude is not required at that stage. This enables the attitude update step to be moved from the beginning to the end of the navigation equations processing cycle, enabling an averaged transport rate to be used for the attitude update:

$$\mathbf{C}_{b}^{n}(+) = \left[\mathbf{I}_3 - \left(\mathbf{\Omega}_{ie}^{e}(-) + \tfrac{1}{2}\mathbf{\Omega}_{en}^{n}(-) + \tfrac{1}{2}\mathbf{\Omega}_{en}^{n}(+)\right)\tau_i\right]\mathbf{C}_{b}^{n}(-)\mathbf{C}_{b+}^{b-}, \qquad (5.77)$$

where $\mathbf{\Omega}_{en}^{n}(+)$ is calculated using $L_b(+)$, $h_b(+)$, and $\mathbf{v}_{eb}^{n}(+)$. Figure 5.8 shows the modified block diagram for the precision local-navigation-frame navigation equations.

Coordinate transformation matrices are orthonormal, (2.17), so the scalar product of any two rows or any two columns should be zero. Orthonormality is

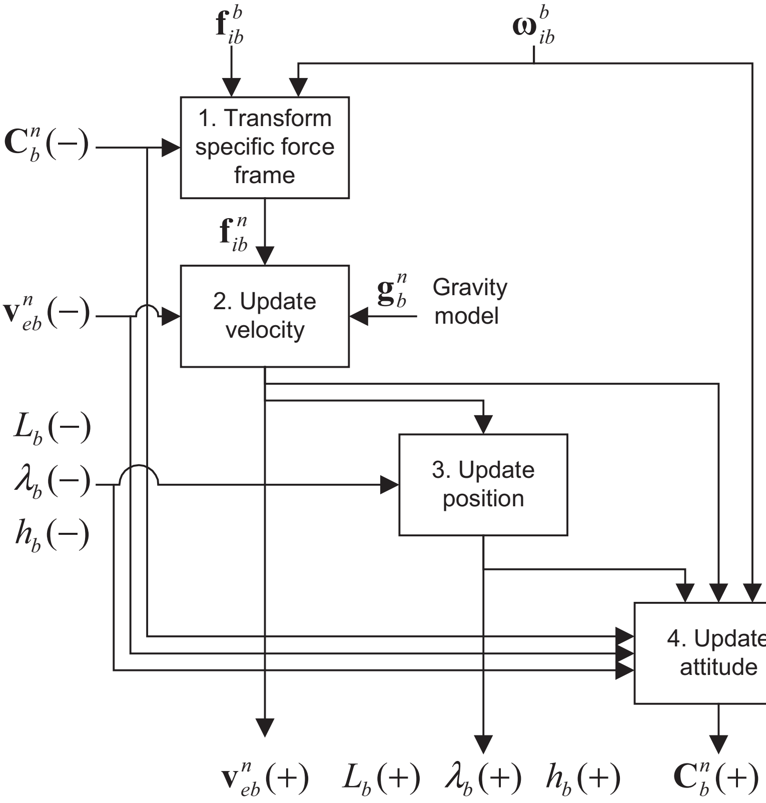

Figure 5.8 Block diagram of precision local-navigation-frame navigation equations.

maintained through exact navigation equations. However, the use of approximations and the presence of computational rounding errors can cause departures from this. Consequently, it can be useful to implement a reorthogonalization and renormalization algorithm at regular intervals.*

Breaking down the coordinate transformation matrix (frames omitted) into three rows,

$$\mathbf{C} = \begin{pmatrix} \mathbf{c}_1^{\mathrm{T}} \\ \mathbf{c}_2^{\mathrm{T}} \\ \mathbf{c}_3^{\mathrm{T}} \end{pmatrix}. \tag{5.78}$$

Orthogonalization is achieved by calculating $\Delta_{ij} = \mathbf{c}_i^{\mathrm{T}}\mathbf{c}_j$ for each pair of rows and apportioning a correction equally between them:†

*This and subsequent paragraphs are based on material written by the author for QinetiQ, so comprise QinetiQ copyright material.

†End of QinetiQ copyright material.

$$\begin{aligned}\mathbf{c}_1(+) &\approx \mathbf{c}_1(-) - \tfrac{1}{2}\Delta_{12}\mathbf{c}_2(-) - \tfrac{1}{2}\Delta_{13}\mathbf{c}_3(-)\\ \mathbf{c}_2(+) &\approx \mathbf{c}_2(-) - \tfrac{1}{2}\Delta_{12}\mathbf{c}_1(-) - \tfrac{1}{2}\Delta_{23}\mathbf{c}_3(-)\,.\\ \mathbf{c}_3(+) &\approx \mathbf{c}_3(-) - \tfrac{1}{2}\Delta_{13}\mathbf{c}_1(-) - \tfrac{1}{2}\Delta_{23}\mathbf{c}_2(-)\end{aligned} \tag{5.79}$$

Normalization is subsequently applied to each row by

$$\begin{aligned}\mathbf{c}_i(+) &= \frac{1}{\sqrt{\mathbf{c}_i^{\mathrm{T}}(-)\mathbf{c}_i(-)}}\mathbf{c}_i(-)\\ &\approx \frac{2}{1+\mathbf{c}_i^{\mathrm{T}}(-)\mathbf{c}_i(-)}\mathbf{c}_i(-)\end{aligned}\,. \tag{5.80}$$

The orthonormalization may also be performed column by column. Note that these corrections work best when the departure from orthonormality is small.

5.5.2 Precision Specific-Force Frame Transformation

The specific force in ECI-frame resolving axes is instantaneously related to that in the body-frame axes by [repeating (5.15)]:

$$\mathbf{f}_{ib}^{i}(t) = \mathbf{C}_b^i(t)\mathbf{f}_{ib}^{b}(t).$$

The IMU outputs the average specific force over the interval t to $t + \tau_i$ and the ECI-axes specific force is similarly averaged. The transformation is thus

$$\mathbf{f}_{ib}^{i} = \bar{\mathbf{C}}_b^i\mathbf{f}_{ib}^{b}, \tag{5.81}$$

where the average coordinate transformation matrix over the time interval is

$$\bar{\mathbf{C}}_b^i = \frac{1}{\tau_i}\int_t^{t+\tau_i}\mathbf{C}_b^i(t')\,dt'. \tag{5.82}$$

Substituting in (5.11), noting that the variation of the angular rate over the integration interval is unknown,

$$\begin{aligned}\bar{\mathbf{C}}_b^i &= \frac{1}{\tau_i}\mathbf{C}_b^i(-)\int_0^{t+\tau_i}\sum_{r=0}^{\infty}\frac{\left\{(t'/\tau_i)\left[\boldsymbol{\alpha}_{ib}^b\wedge\right]\right\}^r}{r!}dt'\\ &= \mathbf{C}_b^i(-)\sum_{r=0}^{\infty}\frac{\left[\boldsymbol{\alpha}_{ib}^b\wedge\right]^r}{(r+1)!}\end{aligned}\,. \tag{5.83}$$

Applying (5.70),

$$\bar{\mathbf{C}}_b^i = \mathbf{C}_b^i(-)\mathbf{C}_{\bar{b}}^{b-}, \quad \mathbf{C}_{\bar{b}}^{b-} = \mathbf{I}_3 + \frac{1-\cos\left|\boldsymbol{\alpha}_{ib}^b\right|}{\left|\boldsymbol{\alpha}_{ib}^b\right|^2}\left[\boldsymbol{\alpha}_{ib}^b \wedge\right] + \frac{1}{\left|\boldsymbol{\alpha}_{ib}^b\right|^2}\left(1 - \frac{\sin\left|\boldsymbol{\alpha}_{ib}^b\right|}{\left|\boldsymbol{\alpha}_{ib}^b\right|}\right)\left[\boldsymbol{\alpha}_{ib}^b \wedge\right]^2. \quad (5.84)$$

Again, this should be replaced with the approximate version whenever $|\boldsymbol{\alpha}_{ib}^b|$ is very small to avoid division by zero.

Substituting this into (5.81) or (5.17), the specific force in ECI-frame resolving axes, $\mathbf{f}_{ib}^i$, or the integrated specific force, $\boldsymbol{\upsilon}_{ib}^i$, may be calculated exactly. Note that $\bar{\mathbf{C}}_b^i$ is not an orthonormal matrix. Therefore, to reverse the transformation described by (5.81), $\bar{\mathbf{C}}_b^i$ must be inverted.

Retaining the first-order approximation for the Earth-rate term, the precise transformation of the specific force to ECEF-frame axes is

$$\mathbf{f}_{ib}^e = \bar{\mathbf{C}}_b^e \mathbf{f}_{ib}^b, \qquad \bar{\mathbf{C}}_b^e = \mathbf{C}_b^e(-)\mathbf{C}_{\bar{b}}^{b-} - \tfrac{1}{2}\boldsymbol{\Omega}_{ie}^e \mathbf{C}_b^e(-)\tau_i. \quad (5.85)$$

To transform the specific force to local-navigation-frame axes, the first-order approximation is also used for the transport-rate term as the velocity at time $t + \tau_i$ has yet to be computed:

$$\mathbf{f}_{ib}^n = \bar{\mathbf{C}}_b^n \mathbf{f}_{ib}^b, \qquad \bar{\mathbf{C}}_b^n = \mathbf{C}_b^n(-)\mathbf{C}_{\bar{b}}^{b-} - \tfrac{1}{2}\left(\boldsymbol{\Omega}_{ie}^n(-) + \boldsymbol{\Omega}_{en}^n(-)\right)\mathbf{C}_b^n(-)\tau_i. \quad (5.86)$$

To transform integrated specific force to ECEF and local-navigation-frame axes, $\bar{\mathbf{C}}_b^e$ and $\bar{\mathbf{C}}_b^n$ are substituted into (5.29) and (5.48), respectively.

The error arising from transforming the specific force as described in Sections 5.2.2, 5.3.2, and 5.4.2 varies approximately as the square of the attitude increment and is maximized where the rotation axis is perpendicular to the direction of the specific force. The maximum fractional error is 8.3×10^{-4} for $|\boldsymbol{\alpha}_{ib}^b| = 0.1$ rad and 2.1×10^{-4} for $|\boldsymbol{\alpha}_{ib}^b| = 0.05$ rad.

5.5.3 Precision Velocity and Position Updates

When the navigation equations are iterated at the IMU output rate and a constant acceleration may be assumed, the ECI-frame velocity and position update equations presented in Sections 5.2.3 and 5.2.4 are exact, except for the variation in gravitation over the update interval, which is small enough to be neglected. However, in the ECEF and local-navigation-frame implementations, exact evaluation of the Coriolis and transport-rate terms requires knowledge of the velocity at the end of the update interval, requiring a recursive solution. For most applications, the first-order approximation in (5.36) and (5.54) is sufficient. However, this may lead to significant errors for high-accuracy, high-dynamic applications. One solution is to predict forward the velocity using previous velocity solutions [2]. A better, but more processor-intensive, solution is a two-step recursive method, shown here for the local-navigation-frame implementation:

$$\begin{aligned}\mathbf{v}_{eb}^{n\prime} &= \mathbf{v}_{eb}^{n}(-) + \left[\mathbf{f}_{ib}^{n} + \mathbf{g}_{b}^{n}\left(L_b(-), h_b(-)\right) - \left(\boldsymbol{\Omega}_{en}^{n}(-) + 2\boldsymbol{\Omega}_{ie}^{n}(-)\right)\mathbf{v}_{eb}^{n}(-)\right]\tau_i \\ \mathbf{v}_{eb}^{n}(+) &= \mathbf{v}_{eb}^{n}(-) + \left\{\begin{array}{l}\mathbf{f}_{ib}^{n} + \mathbf{g}_{b}^{n}\left(L_b(-), h_b(-)\right) - \frac{1}{2}\left[\boldsymbol{\Omega}_{en}^{n}(-) + 2\boldsymbol{\Omega}_{ie}^{n}(-)\right]\mathbf{v}_{eb}^{n}(-) \\ -\frac{1}{2}\left[\boldsymbol{\Omega}_{en}^{n}(L_b(-), h_b(-),\, \mathbf{v}_{eb}^{n\prime}) + 2\boldsymbol{\Omega}_{ie}^{n}(-)\right]\mathbf{v}_{eb}^{n\prime}\end{array}\right\}\tau_i\end{aligned} \quad . \qquad (5.87)$$

Provided they are iterated at the same rate as the velocity update, the ECI- and ECEF-frame position updates introduce no further approximations beyond those made in the velocity update, while the effect of the meridian radius of curvature approximation in (5.56) is negligible.

When the latitude and longitude are updated using the coordinate transformation matrices from a local-navigation or wander-azimuth frame to an ECEF frame, greater accuracy may be obtained using Rodrigues' formula:

$$\begin{aligned}\mathbf{C}_{n}^{e}(+) &= \mathbf{C}_{n}^{e}(-)\left(\mathbf{I}_3 + \frac{\sin\left|\boldsymbol{\alpha}_{en}^{n}\right|}{\left|\boldsymbol{\alpha}_{en}^{n}\right|}\left[\boldsymbol{\alpha}_{en}^{n}\wedge\right] + \frac{1-\cos\left|\boldsymbol{\alpha}_{en}^{n}\right|}{\left|\boldsymbol{\alpha}_{en}^{n}\right|^2}\left[\boldsymbol{\alpha}_{en}^{n}\wedge\right]^2\right) \\ \mathbf{C}_{w}^{e}(+) &= \mathbf{C}_{w}^{e}(-)\left(\mathbf{I}_3 + \frac{\sin\left|\boldsymbol{\alpha}_{ew}^{w}\right|}{\left|\boldsymbol{\alpha}_{ew}^{w}\right|}\left[\boldsymbol{\alpha}_{ew}^{w}\wedge\right] + \frac{1-\cos\left|\boldsymbol{\alpha}_{ew}^{w}\right|}{\left|\boldsymbol{\alpha}_{ew}^{w}\right|^2}\left[\boldsymbol{\alpha}_{ew}^{w}\wedge\right]^2\right)\end{aligned}, \qquad (5.88)$$

where

$$\begin{aligned}\boldsymbol{\alpha}_{en}^{n} &= \int_{t}^{t+\tau_i} \boldsymbol{\omega}_{en}^{n}(t')\,dt' \approx \tfrac{1}{2}\left(\boldsymbol{\omega}_{en}^{n}(-) + \boldsymbol{\omega}_{en}^{n}(+)\right)\tau_i \\ \boldsymbol{\alpha}_{ew}^{w} &= \int_{t}^{t+\tau_i} \boldsymbol{\omega}_{ew}^{w}(t')\,dt' \approx \tfrac{1}{2}\left(\boldsymbol{\omega}_{ew}^{w}(-) + \boldsymbol{\omega}_{ew}^{w}(+)\right)\tau_i\end{aligned} \qquad (5.89)$$

and approximate versions (see Section 5.5.1) should be used whenever $|\boldsymbol{\alpha}_{en}^{n}|$ or $|\boldsymbol{\alpha}_{ew}^{w}|$ is small to avoid division by zero.

Gravity model limitations can contribute several hundred meters to the position error over the course of an hour. Therefore, where precision inertial sensors and navigation equations are used, navigation accuracy can be significantly improved by using a precision gravity model (see Section 2.4.7) [6]. Alternatively, a gravity gradiometer (Section 13.4.1) can be used to measure gravitational variations in real time [7].

5.5.4 Effects of Sensor Sampling Interval and Vibration

The inertial sensor measurements enable the average specific force and angular rate over the sensor sampling interval, τ_i, to be determined. However, they do not give information on the variation in specific force and angular rate over that interval. Figure 5.9 shows different specific force or angular rate profiles that produce the same sensor output. Inertial navigation processing typically operates under the

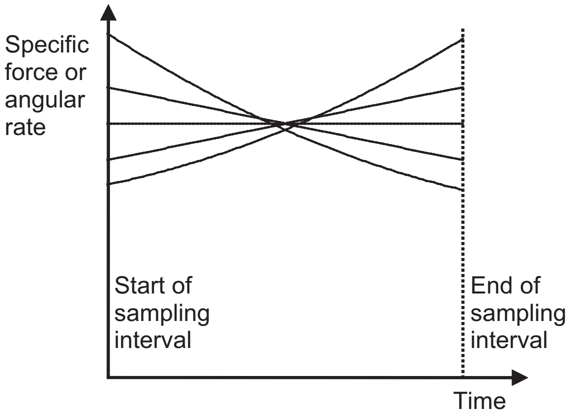

Figure 5.9 Different specific force or angular rate profiles producing the same sensor output.

assumption that the specific force and angular rate, as resolved in the body frame, are constant over the sampling interval. Figure 5.10 illustrates this.

If the direction of rotation remains constant over the gyro sampling interval, the same attitude update will be obtained from the average angular rate as from the true angular rate. However, if the direction of rotation changes, errors will occur because successive rotations about different directions do not commute (see Section 2.2).

Similarly, if the attitude of the IMU body remains constant over the accelerometer sampling interval, the same velocity update will be obtained from the average specific force as from the true specific force. However, if the body is rotating, any unknown variation in the specific force will result in an error in the transformation of the specific force into the resolving axes used for the velocity computation. A similar error will occur where the angular rate is changing even if the specific force is constant. Note also that assuming a constant acceleration in the presence of jerk (rate of change of acceleration) leads to an error in the position update.

Consider three examples, all assuming a 100-Hz IMU sampling rate. First, a 1 rad s^{-1} angular rate is combined with an angular acceleration of 1 rad s^{-2} about

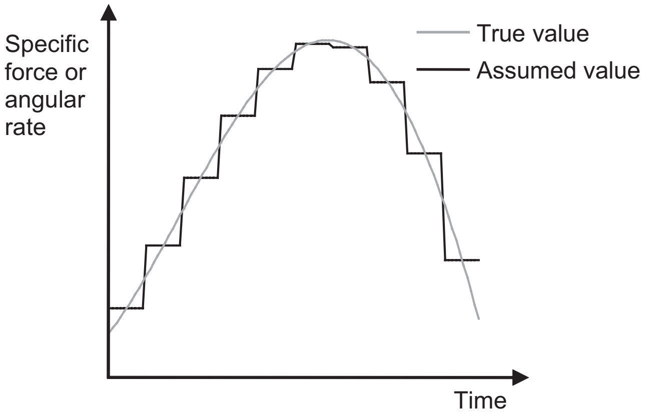

Figure 5.10 True and assumed sensor outputs.

a perpendicular axis. This leads to an angular rate error of 1.7×10^{-5} rad s^{-1} (3.5 ° hr^{-1}) about the mutually perpendicular axis. Second, a combination of a 1 rad s^{-2} angular acceleration with a specific force along a perpendicular axis of 10 m s^{-2} leads to a specific force frame transformation error of 8.3×10^{-5} m s^{-2} (8.5 μg) along the mutually perpendicular axis. Finally, the combination of a 100 m s^{-3} jerk with an angular rate of 1 rad s^{-1} about a perpendicular axis leads to a specific force frame transformation error along the mutually perpendicular axis of 8.3×10^{-4} m s^{-2} (985 μg). When such conditions result from dynamic maneuvers of the host vehicle, the duration over which the specific force and angular rate errors apply will typically be short, while successive maneuvers will often produce canceling errors. However, vibration-induced errors can have a more significant impact on inertial navigation performance.

The effects of vibration may be illustrated by the cases of coning and sculling motion. Coning motion is synchronized angular oscillation about two orthogonal axes as shown in Figure 5.11. Where there is a phase difference between the two oscillations, the resultant axis of rotation precesses, describing a cone-like surface. Note that mechanical dithering of an RLG triad (see Section 4.2.1.1) induces coning motion [8].

If the output of a triad of gyroscopes is integrated over a period, τ, in the presence of coning motion of angular frequency, ω_c, and angular amplitudes, $\boldsymbol{\theta}_i$ and $\boldsymbol{\theta}_j$, with a phase difference, ϕ, between the two axes, it can be shown [1] that a false rotation, $\delta\boldsymbol{\omega}_c$, is sensed about the axis orthogonal to $\boldsymbol{\theta}_i$ and $\boldsymbol{\theta}_j$, where

$$\delta\boldsymbol{\omega}_c = \omega_c \boldsymbol{\theta}_i \wedge \boldsymbol{\theta}_j \sin\phi \left(1 - \frac{\sin\omega_c\tau}{\omega_c\tau}\right). \tag{5.90}$$

This arises due to the difference between the actual and assumed order of rotation over the integration period. The coning error, $\delta\boldsymbol{\omega}_c$, does not oscillate. Therefore, the attitude solution drifts under a constant coning motion. The higher the frequency of the coning motion and the longer the gyro outputs are integrated, the larger the drift will be. For example, if the coning amplitude is 1 mrad, the frequency is 100 rad s^{-1} (15.9 Hz), and the integration interval is 0.01 second, the maximum coning error is 1.59×10^{-5} rad s^{-1} (3.3 ° hr^{-1}). For a vibration frequency of 200 rad s^{-1}, the maximum error is 1.09×10^{-4} rad s^{-1} (22.5 ° hr^{-1}). These values assume the use of exact navigation equations. Much larger coning errors can occur where approximations are made, particularly in the attitude update step.

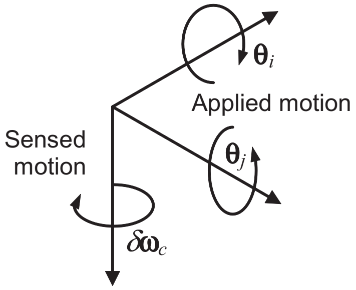

Figure 5.11 Coning motion. (*From:* [9]. ©2002 QinetiQ Ltd. Reprinted with permission.)

Sculling motion is synchronized angular oscillation about one axis and linear oscillation about an orthogonal axis as shown in Figure 5.12. This results in an error in the output of an accelerometer triad. If the angular frequency is ω_s and the acceleration amplitude is $\mathbf{a}_j$, a false acceleration, $\delta\mathbf{a}_s$, is sensed about the axis orthogonal to $\boldsymbol{\theta}_i$ and a_j. From [1],

$$\delta\mathbf{a}_s = \tfrac{1}{2}\boldsymbol{\theta}_i \wedge \mathbf{a}_j \cos\phi\left(1 - \frac{\sin\omega_s\tau}{\omega_s\tau}\right). \tag{5.91}$$

Similarly, the sculling error, $\delta\mathbf{a}_s$, does not oscillate so the navigation solution drifts under constant sculling motion. Again, the resulting acceleration error is larger for longer integration times and higher sculling frequencies. For example, if the angular vibration amplitude is 1 mrad, the linear vibration amplitude is 1 mm, the frequency is 100 rad s^{-1} (15.9 Hz), and the integration interval is 0.01 second, the maximum sculling error is 7.9×10^{-4} m s^{-2} (79 μg). For a vibration frequency of 200 rad s^{-1}, the maximum error is 1.09×10^{-2} m s^{-1} (1.1 mg). Again, larger errors can occur when approximate navigation equations are used.

Although long periods of in-phase coning and sculling rarely occur in real systems, the navigation solution can still be significantly degraded by the effects of orthogonal vibration modes. Therefore, coning and sculling motion provides a useful test case for inertial navigation equations. The extent to which the navigation equations design must protect against the effects of vibration depends on both the accuracy requirements and the vibration environment. An example of a high-vibration environment is an aircraft wing pylon, where a guided weapon or sensor pod may be mounted.

The coning and sculling errors, together with the other errors that can arise from averaging specific force and angular rate, vary approximately as the square of the averaging interval. Consequently, when the navigation equations are iterated at a lower rate than the IMU output to reduce the processor load (see Section 5.5.5), successive IMU outputs should not be simply averaged.

The angular rate measurements should be combined using a method that minimizes coning errors. When the integration interval for the attitude update comprises n IMU output intervals, an exact attitude update matrix may be constructed by multiplying the attitude update matrices for each interval:

$$\mathbf{C}_{b+}^{b-} = \exp\left[\boldsymbol{\alpha}_{ib,1}^{b} \wedge\right]\exp\left[\boldsymbol{\alpha}_{ib,2}^{b} \wedge\right]\ldots\exp\left[\boldsymbol{\alpha}_{ib,n}^{b} \wedge\right], \tag{5.92}$$

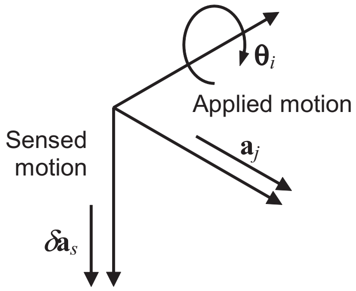

Figure 5.12 Sculling motion. (*From:* [9]. ©2002 QinetiQ Ltd. Reprinted with permission.)

where

$$\boldsymbol{\alpha}^b_{ib,j} = \int_{t+(j-1)\tau_i/n}^{t+j\tau_i/n} \boldsymbol{\omega}^b_{ib}(t')\,dt'. \tag{5.93}$$

Implementing (5.92) as it stands offers no computational saving over performing the attitude update at the IMU rate. From (2.43), the attitude update matrix may be expressed in terms of a rotation vector [10]:

$$\mathbf{C}^{b-}_{b+} = \exp\left[\boldsymbol{\rho}_{b-b+}\wedge\right]. \tag{5.94}$$

Note that the body-frame rotation vector, $\boldsymbol{\rho}_{b-b+}$, is equal to the attitude increment of the body frame with respect to inertial space in body-frame axes, $\boldsymbol{\alpha}^b_{ib}$, over the same time interval. Thus,

$$\boldsymbol{\rho}_{b-b+} = \int_{t}^{t+\tau_i} \boldsymbol{\omega}^b_{ib}(t')\,dt'. \tag{5.95}$$

Note, however, that rotation vectors and attitude increments are not the same in general.

As the direction of rotation varies between successive measurements, the rotation vector is not simply the sum of the attitude increments. In physical terms, this is because the resolving axes vary between successive attitude increments. In mathematical terms, the skew-symmetric matrices of successive attitude increments do not commute.

From [10], the rate of change of the rotation vector varies with the angular rate as

$$\dot{\boldsymbol{\rho}}_{b-b+} = \boldsymbol{\omega}^b_{ib} + \frac{1}{2}\boldsymbol{\rho}_{b-b+}\wedge\boldsymbol{\omega}^b_{ib} + \frac{1}{\left|\boldsymbol{\rho}_{b-b+}\right|^2}\left[1 - \frac{\left|\boldsymbol{\rho}_{b-b+}\right|\sin\left|\boldsymbol{\rho}_{b-b+}\right|}{2\left(1-\cos\left|\boldsymbol{\rho}_{b-b+}\right|\right)}\right]\boldsymbol{\rho}_{b-b+}\wedge\boldsymbol{\rho}_{b-b+}\wedge\boldsymbol{\omega}^b_{ib}. \tag{5.96}$$

From [2, 11], a second-order approximation incorporating only the first two terms of (5.96) gives the following solution:

$$\boldsymbol{\rho}_{b-b+} \approx \sum_{j=1}^{n}\boldsymbol{\alpha}^b_{ib,j} + \frac{1}{2}\sum_{j=1}^{n-1}\sum_{k=j+1}^{n}\boldsymbol{\alpha}^b_{ib,j}\wedge\boldsymbol{\alpha}^b_{ib,k}. \tag{5.97}$$

Note that, where sufficient processing capacity is available, it is both simpler and more accurate to iterate the attitude update at the IMU output rate.

Similarly, when the specific force in the resolving axes used for the velocity update is integrated over more than one IMU output interval, the specific-force transformation should account for the fact that each successive IMU specific-force measurement may be resolved about a different set of axes as the body-frame orientation changes. This minimizes the sculling error. A second-order transformation and summation of n successive IMU-specific force measurements into an ECI frame is, from [1, 2, 11],

$$\boldsymbol{\upsilon}^i_{ib,\Sigma} \approx \mathbf{C}^i_b(-)\left[\sum_{j=1}^{n}\boldsymbol{\upsilon}^b_{ib,j} + \frac{1}{2}\sum_{j=1}^{n}\sum_{k=1}^{n}\boldsymbol{\alpha}^b_{ib,j}\wedge\boldsymbol{\upsilon}^b_{ib,k} + \frac{1}{2}\sum_{j=1}^{n-1}\sum_{k=j+1}^{n}\left(\boldsymbol{\alpha}^b_{ib,j}\wedge\boldsymbol{\upsilon}^b_{ib,k} - \boldsymbol{\alpha}^b_{ib,k}\wedge\boldsymbol{\upsilon}^b_{ib,j}\right)\right]. \tag{5.98}$$

where $\boldsymbol{\upsilon}^b_{ib,j}$ and $\boldsymbol{\alpha}^b_{ib,j}$ are the jth integrated-specific-force and attitude-increment outputs from the IMU, and $\boldsymbol{\upsilon}^i_{ib,\Sigma}$ is the summed integrated specific force in ECI resolving axes. Again, where there is sufficient processing capacity, it is simpler and more accurate to iterate the specific-force transformation at the IMU update rate.

The higher-order terms in (5.97) and (5.98) are sometimes known as coning and sculling corrections. When an IMU samples the gyros and accelerometers at a higher rate than it outputs angular rate and specific force, coning and sculling corrections may be applied by its processor prior to output.

When coning and sculling corrections are not applied within the IMU and the frequency of the vibration is less than half of the IMU output rate (i.e., the Nyquist rate), further reductions in the coning and sculling errors may be obtained by interpolating the IMU measurements to a higher rate. This makes use of earlier and, sometimes later, measurements to estimate the variation in specific force and angular rate over the sampling interval and may be performed in either the time domain or the frequency domain. Figure 5.13 illustrates this, noting that the average value of the interpolated measurement over each original measurement interval must equal the original measurement. The measurements may then be recombined using (5.93) to (5.98). Note that a processing lag is introduced if later measurements are used in the interpolation process. Also, the signal variation must exceed the IMU noise and quantization levels (see Section 4.4.3) for the interpolation to be useful; this is a particular issue for consumer-grade MEMS sensors.

When the position update interval is longer than the interval over which the IMU measurements are assumed to be constant, the assumption that the acceleration is constant over the update interval will introduce a correctable position error. This error will typically be small compared to the position accuracy requirement and/or other error sources. However, where necessary, it may be eliminated by applying a scrolling correction as described in [2, 11].

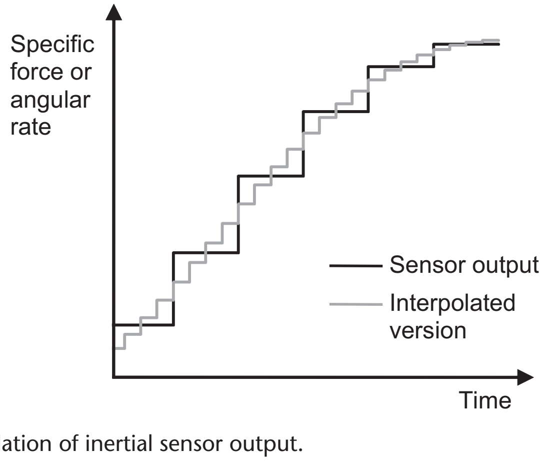

Figure 5.13 Interpolation of inertial sensor output.

5.5.5 Design Tradeoffs

The design of a set of inertial navigation equations is a tradeoff among accuracy, processing efficiency, and complexity. It is possible to optimize two of these, but not all three. In determining the accuracy requirements, it is important to consider the navigation system as a whole. For example, where the inertial sensors are relatively poor, an improvement in the accuracy of the navigation equations may have negligible impact on overall performance. Another consideration is the degree to which integration with other navigation sensors can correct the errors of the INS [12]. This can lead to a more demanding requirement for the attitude update accuracy than for the position and velocity as the latter are easier to correct using other sensors (see Section 14.2.1).

Traditionally, the accuracy requirements for inertial navigation have been high, as INS with high-quality inertial sensors have been used for sole-means navigation in the horizontal axes, or with infrequent position updates, for periods of hours. Until the 1990s, processing power was also at a premium. Hence considerable effort was expended developing highly accurate and highly efficient, but also highly complex, navigation algorithms (e.g., [2]). However, today, a faster processor can often be more cost effective than expending a large amount of effort designing, implementing, and debugging complex navigation equations.

The accuracy of the navigation equations is a function of three factors: the iteration rate, the nature of the approximations made, and the dynamic and vibration environment. The greater the level of dynamics or vibration, the greater the impact on navigation solution accuracy of an approximation in the navigation equations or a change in the iteration rate. At a given level of dynamics or vibration, the impact of an approximation is greater where the iteration rate is lower (i.e., the integration step is larger).

Different approximations in different stages of the navigation equations have differing impacts on the overall position, velocity, and attitude errors, depending on the magnitude and type of the dynamics and vibration. For example, in the ECEF-frame and local-navigation-frame implementations, the Earth-rate, transport-rate, and Coriolis terms tend to be much smaller than the terms derived from the accelerometer and gyro measurements. Consequently, approximating these terms and/or calculating them at a lower iteration rate will have less impact on overall navigation accuracy, providing an opportunity to improve the processing efficiency. A common approach is to combine successive IMU outputs using (5.94), (5.97), and (5.98) and then iterate precision inertial navigation equations (Sections 5.5.1 to 5.5.3) at a lower rate, for example, 50–200 Hz [2].

Section E.8 of Appendix E on the CD discusses a number of iteration rate issues, including using different iteration rates for different stages, using numerical integration, and iterating approximate forms of the navigation equations faster than the IMU output rate.

5.6 Initialization and Alignment

As Figure 5.3 shows, an INS calculates a navigation solution by integrating the inertial sensor measurements. Thus, each iteration of the navigation equations uses the previous navigation solution as its starting point. Therefore, before an INS can be used to provide a navigation solution, that navigation solution must be initialized.

Initial position and velocity must be provided from external information. Attitude may be initialized either from an external source or by sensing gravity and the Earth's rotation.[‡] The attitude initialization process is also known as alignment because, in a platform INS (Section E.5 of Appendix E on the CD), the inertial instruments are physically aligned with the axes of a local navigation frame.

The initialization is often followed by a period of calibration when stationary or against an external reference, typically lasting a few minutes. This is known as fine alignment, as its main role is to reduce the attitude initialization errors.

5.6.1 Position and Velocity Initialization

The INS position and velocity must be initialized using external information. When the host vehicle has not moved since the INS was last used, the last known position may be stored and used for initialization. However, an external position reference must be introduced at some point to prevent the navigation solution drift accumulating over successive periods of operation.

INS position may be initialized from another navigation system. This may be another INS, GNSS user equipment, or terrestrial radio navigation user equipment. Alternatively, the INS may be placed near a presurveyed point, or range and/or bearing measurements to known landmarks taken. In either case, the lever arm between the INS and the position reference must be measured. If this is only known in the body frame, the INS attitude will be required to transform the lever arm to the same coordinate frame as the position fix (see Section 2.5.5).

Velocity may be initialized simply by maintaining the INS stationary with respect to the Earth. Alternatively, another navigation system, such as GNSS, Doppler radar, or another INS, may be used as a reference. In that case, the lever arm and angular rate are required to calculate the lever arm velocity.

Further problems for velocity initialization are disturbance, vibration, and flexure. For example, when the INS is assumed to be stationary with respect to the Earth, the host vehicle could be disturbed by the wind or by human activity, such as refueling and loading. For ships and boats, water motion is also an issue. For in-motion initialization, the lever arm between the INS and the reference navigation system can be subject to flexure and vibration. The solution is to take initialization measurements over a few seconds and average them. Position can also be affected by flexure and vibration, but the magnitude is usually less than the accuracy required.

In the MATLAB INS/GNSS integration software on the CD, the inertial position and velocity solutions are initialized from the GNSS solution. For stand-alone inertial navigation, the MATLAB function, Initialize_NED, simply initializes the navigation solution to the truth offset by user-specified errors.

5.6.2 Attitude Initialization

When the INS is stationary, self-alignment can be used to initialize the roll and pitch with all but the poorest inertial sensors. However, accurate self-alignment of the

[‡] This paragraph, up to this point, is based on material written by the author for QinetiQ, so comprises QinetiQ copyright material.

heading requires aviation-grade gyros or better. Heading is often initialized using a magnetic compass, described in Section 6.1.1.

When the INS is initialized in motion, another navigation system must provide an attitude reference. For guided weapons, the host vehicle's INS is generally used. Multiple-antenna GNSS user equipment can also be used to measure attitude. However, this is very noisy unless long baselines and/or long averaging times are used, as described in Section 10.2.5. Another option for some applications is the star imager, described in Section 13.3.7. In all cases, the accuracy of the attitude initialization depends on how well the relative orientation of the initializing INS and the reference navigation system is known, as well as on the accuracy of the reference attitude. If there is significant flexure in the lever arm between the two systems, such as that which occurs for equipment mounted on an aircraft wing, the relative orientation may only be known to a few tens of milliradians (a degree or two).

For IMUs attached to most land vehicles, it can be assumed that the direction of travel defines the body x-axis except when the vehicle is turning (see Section 6.1.4). This enables a trajectory measured by a positioning system, such as GNSS, to be used to initialize the pitch and heading attitudes. When a portable IMU is used, there is no guarantee that the body x-axis will be aligned with the direction of travel. On a land vehicle, the normal direction of travel can be identified from the acceleration and deceleration that occurs when the vehicle starts and stops, which is normally accompanied by forward motion [13]. Once the IMU is aligned with the vehicle, its heading may be derived from the trajectory.

For aircraft and ships the direction of travel will only provide a rough attitude initialization as sideslip, due to wind or sea motion, results in an offset between the heading and the trajectory, while aircraft pitch is defined by the angle of attack needed to obtain lift and ship pitch oscillates due to the sea state. Trajectory-based heading alignment is thus context dependent.

Other alignment methods include memory, whereby the attitude is assumed to be the same as when the INS was last used; using a prealigned portable INS to transfer the attitude solution from a ready room; and aligning the host vehicle with a known landmark, such as a runway [14].

Self-alignment comprises two processes: a leveling process, which initializes the roll and pitch attitudes, and a gyrocompassing process, which initializes the heading. The leveling is normally performed first.

The principle behind *leveling* is that, when the INS is stationary (or traveling at constant velocity), the only specific force sensed by the accelerometers is the reaction to gravity, which is approximately in the negative down direction of a local navigation frame at the Earth's surface. Figure 5.14 illustrates this. Thus the attitude, $\mathbf{C}_b^n$, can be estimated by solving*

$$\mathbf{f}_{ib}^b = \mathbf{C}_n^b \mathbf{g}_b^n(L_b, h_b), \tag{5.99}$$

given $\mathbf{a}_{eb}^\gamma = 0$. Taking the third column of $\mathbf{C}_n^b$, given by (2.22), (5.99) can be expressed in terms of the pitch, θ_{nb}, and roll, ϕ_{nb}, Euler angles:

*This and subsequent paragraphs are based on material written by the author for QinetiQ, so comprise QinetiQ copyright material.

$$\begin{pmatrix} f_{ib,x}^{b} \\ f_{ib,y}^{b} \\ f_{ib,z}^{b} \end{pmatrix} = \begin{pmatrix} \sin\theta_{nb} \\ -\cos\theta_{nb}\sin\phi_{nb} \\ -\cos\theta_{nb}\cos\phi_{nb} \end{pmatrix} g_{b,D}^{n}(L_b, h_b), \tag{5.100}$$

where $g_{b,D}^{n}$ is the down component of the acceleration due to gravity. This solution is overdetermined. Therefore, pitch and roll may be determined without knowledge of gravity, and hence the need for position, using[†]

$$\theta_{nb} = \arctan\left(\frac{f_{ib,x}^{b}}{\sqrt{f_{ib,y}^{b\;2} + f_{ib,z}^{b\;2}}}\right), \qquad \phi_{nb} = \arctan_2\left(-f_{ib,y}^{b}, -f_{ib,z}^{b}\right), \tag{5.101}$$

noting that a four-quadrant arctangent function must be used for roll.

When the INS is absolutely stationary, the attitude initialization accuracy is determined only by the accelerometer errors. For example, a 1-mrad roll and pitch accuracy is obtained from accelerometers accurate to 10^{-3} g. Disturbing motion, such as mechanical vibration, wind effects, and human activity, disrupts the leveling process. However, if the motion averages out over time, its effects on the leveling process may be mitigated simply by time-averaging the accelerometer measurements over a few seconds.

The pitch and roll initialization errors from leveling are then

$$\begin{aligned} \delta\theta_{nb} &= \frac{\left(f_{ib,y}^{b\;2} + f_{ib,z}^{b\;2}\right)\delta f_{ib,x}^{b} - f_{ib,x}^{b} f_{ib,y}^{b}\delta f_{ib,y}^{b} - f_{ib,x}^{b} f_{ib,z}^{b}\delta f_{ib,z}^{b}}{\left(f_{ib,x}^{b\;2} + f_{ib,y}^{b\;2} + f_{ib,z}^{b\;2}\right)\sqrt{f_{ib,y}^{b\;2} + f_{ib,z}^{b\;2}}} \\ \delta\phi_{nb} &= \frac{f_{ib,z}^{b}\delta f_{ib,y}^{b} - f_{ib,y}^{b}\delta f_{ib,z}^{b}}{f_{ib,y}^{b\;2} + f_{ib,z}^{b\;2}} \end{aligned}, \tag{5.102}$$

where the accelerometer error model is described in Section 4.4.6.

The principle behind gyrocompassing is that, when the INS is stationary (or traveling in a straight line in an inertial frame), the only rotation it senses is that of the Earth, which is in the *z* direction of an ECEF frame. Measuring this rotation in the body frame enables the heading to be determined, except at or very near to the poles, where the rotation axis and gravity vector coincide. Figure 5.15 illustrates the concept. There are two types of gyrocompassing, direct and indirect.

Direct gyrocompassing measures the Earth rotation directly using the gyros. The attitude, $\mathbf{C}_b^n$, may be obtained by solving

$$\boldsymbol{\omega}_{ib}^{b} = \mathbf{C}_n^b \mathbf{C}_e^n(L_b, \lambda_b)\begin{pmatrix} 0 \\ 0 \\ \omega_{ie} \end{pmatrix}, \tag{5.103}$$

[†] End of QinetiQ copyright material.

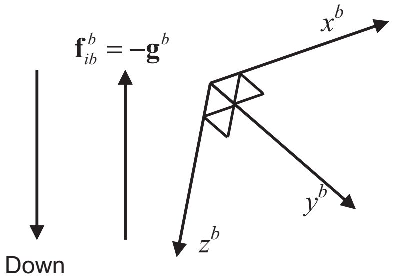

Figure 5.14 Principle of leveling. (*From:* [9]. © 2002 QinetiQ Ltd. Reprinted with permission.)

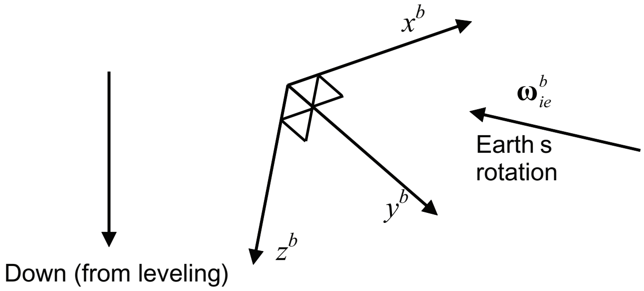

Figure 5.15 Principle of gyrocompassing. (*From:* [9]. © 2002 QinetiQ Ltd. Reprinted with permission.)

given that $\boldsymbol{\omega}_{eb}^{\gamma} = 0$. Substituting in (2.150) and rearranging,

$$\begin{pmatrix} \cos L_b \omega_{ie} \\ 0 \\ -\sin L_b \omega_{ie} \end{pmatrix} = \mathbf{C}_b^n \boldsymbol{\omega}_{ib}^b, \tag{5.104}$$

When the roll and pitch have already been obtained from leveling, the knowledge that the Earth's rotation vector has no east component in a local navigation frame can be used to remove the need for prior position knowledge. Thus, applying (2.24) to (5.104) and taking the second row give the heading Euler angle, ψ_{nb}, in terms of the roll, pitch, and gyro measurements:

$$\begin{aligned} \psi_{nb} &= \arctan_2\left(\sin\psi_{nb}, \cos\psi_{nb}\right) \\ \sin\psi_{nb} &= -\omega_{ib,y}^b \cos\phi_{nb} + \omega_{ib,z}^b \sin\phi_{nb} \\ \cos\psi_{nb} &= \omega_{ib,x}^b \cos\theta_{nb} + \omega_{ib,y}^b \sin\phi_{nb} \sin\theta_{nb} + \omega_{ib,z}^b \cos\phi_{nb} \sin\theta_{nb} \end{aligned} . \tag{5.105}$$

Again, a four-quadrant arctangent function must be used. Equations for performing leveling and direct gyrocompassing in one step are presented in a number of texts [1, 15, 16]. However, these require knowledge of the latitude.

Example 5.3 on the CD illustrates both leveling and direct gyrocompassing in the presence of accelerometer and gyro errors and may be edited using Microsoft Excel.

In the presence of angular disturbing motion, the gyro measurements used for direct gyrocompassing must be time averaged. However, even small levels of angular vibration will be much larger than the Earth-rotation rate. Therefore, if the INS is mounted on any kind of vehicle, an averaging time of many hours can be required. Thus, the application of direct gyrocompassing is limited.

Indirect gyrocompassing uses the gyros to compute a relative attitude solution, which is used to transform the specific-force measurements into inertial resolving axes. The direction of the Earth's rotation is then obtained from rotation about this axis of the inertially resolved gravity vector. Over a sidereal day, this vector forms a cone, while its time derivative rotates within the plane perpendicular to the Earth's rotation axis. Figure 5.16 illustrates this.

The process typically takes 2 to 10 minutes, depending on the amount of linear vibration and disturbance and the accuracy required. Indirect gyrocompassing is typically combined with fine alignment. A suitable quasi-stationary alignment algorithm is described in Section 15.2.

The accuracy of both gyrocompassing methods depends on gyro performance. Given that $\omega_{ie} \approx 7\times10^{-5}$ rad s^{-1}, to obtain a 1-mrad heading initialization at the equator, the gyros must be accurate to around 7×10^{-8} rad s^{-1} or about 0.01 ° hr^{-1}. Only aviation- and marine-grade gyros are this accurate. INSs with gyro biases exceeding about 5°/hr are not capable of gyrocompassing at all. Note that the accuracy of the roll and pitch initialization also affects the heading initialization.

The heading initialization error from gyrocompassing [17] is

$$\delta\psi_{nb} = -\frac{\delta f^{b}_{ib,y}}{g^{n}_{b,D}}\tan L_b + \frac{\delta\omega^{b}_{ib,y}}{\omega_{ie}}\sec L_b, \qquad (5.106)$$

where the accelerometer and gyro error models are presented in Section 4.4.6.

In principle, leveling and gyrocompassing techniques can be performed when the INS is not stationary if the acceleration, $\boldsymbol{\alpha}^{b}_{eb}$, and angular rate, $\boldsymbol{\omega}^{b}_{eb}$, with respect to the Earth are provided by an external sensor.[‡] However, as the relative orientation of the external sensor must be known, this would be no more accurate than simply using the external sensor as an attitude reference.

5.6.3 Fine Alignment

Most inertial navigation applications require attitude to 1 mrad or better, if only to minimize position and velocity drift. Most attitude initialization techniques do not achieve this accuracy. It is therefore necessary to follow the initialization with a period of attitude calibration known as fine alignment.[*]

In fine alignment techniques, the residual attitude errors are sensed through the growth in the velocity errors. For example, a 1-mrad pitch or roll attitude error

[‡] This paragraph, up to this point, is based on material written by the author for QinetiQ, so comprises QinetiQ copyright material.

[*] This and subsequent paragraphs are based on material written by the author for QinetiQ, so comprise QinetiQ copyright material.

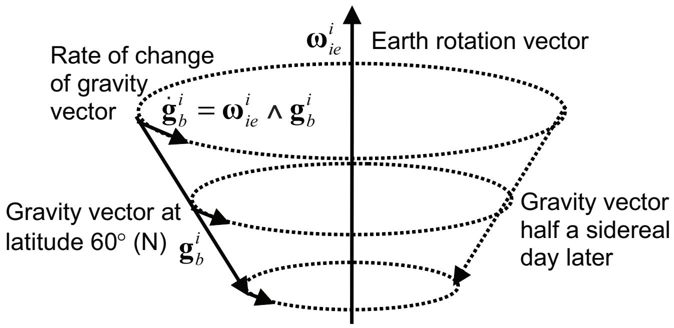
$\boldsymbol{\omega}_{ie}^{i}$
Earth rotation vector
Rate of change of gravity vector
$\dot{\mathbf{g}}_{b}^{i} = \boldsymbol{\omega}_{ie}^{i} \wedge \mathbf{g}_{b}^{i}$
Gravity vector at latitude 60° (N)
$\mathbf{g}_{b}^{i}$
Gravity vector half a sidereal day later

Figure 5.16 Earth rotation and gravity vectors resolved in ECI-frame axes.

will cause the horizontal velocity error to grow at a rate of ~10 mm s^{-2} due to false resolving of gravity.

There are three main fine alignment techniques, each providing a different reference to align against. *Quasi-stationary alignment* assumes that the position has been initialized and that the INS is stationary with respect to the Earth and uses zero velocity updates (ZVUs) or integrals thereof. *GNSS alignment*, or INS/GNSS integration, uses position and velocity derived from GNSS and can operate during the navigation phase as well as the alignment phase. Finally, *transfer alignment* uses position or velocity, and sometimes attitude, from another INS or INS/GNSS. It is generally used for aligning a guided-weapon INS between power-up and launch.† Alternatively, any other position-fixing or dead-reckoning technology, or combination thereof, that provides a 3-D position and velocity solution may be used as the reference for fine alignment. For foot-mounted inertial navigation, a ZVU can be performed during the stance phase of every step.

In all cases, measurements of the difference between the INS outputs and the reference are input to an estimation algorithm, such as a Kalman filter, which calibrates the velocity, attitude, and sometimes the position, depending on which measurements are used. Figure 5.17 illustrates this. Inertial instrument errors, such as accelerometer and gyro biases, are often estimated as well. However, when the INS is stationary, the effects of instrument errors cannot be fully separated from the attitude errors. For example, a 10 mm s^{-2} accelerometer bias can have the same effect on velocity as a 1-mrad attitude error. To separately observe these errors, maneuvers must be performed as discussed in Section 14.2.1. For example, if the INS is rotated, a given accelerometer error will have the same effect on velocity as a different attitude error. In quasi-stationary alignment, maneuvers are generally limited to heading changes, with the alignment process suspended during host vehicle maneuvers. For GNSS and transfer alignment, the maneuvers are limited only by the capabilities of the host vehicle. Even with maneuvers, there will still be some correlation between the residual INS errors following fine alignment.‡

†End of QinetiQ copyright material.

‡This paragraph, up to this point, is based on material written by the author for QinetiQ, so comprises QinetiQ copyright material.

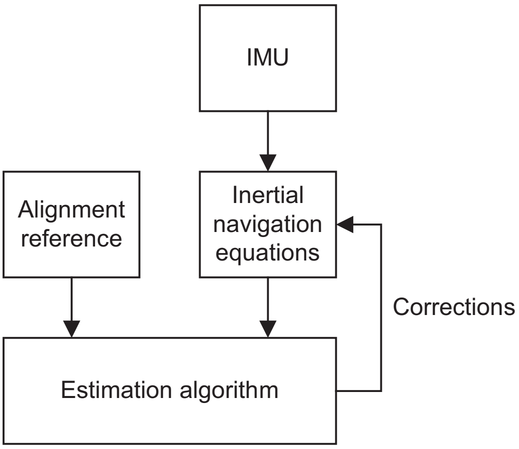

Figure 5.17 INS fine alignment architecture.

INS/GNSS integration algorithms are described in detail in Chapter 14, while quasi-stationary, transfer alignment, and ZVUs are described in Chapter 15. The use of other navigation systems to calibrate INS errors is described in Chapter 16, noting that an error-state integration architecture with the INS as the reference should be used.

The main differences between the techniques are the types of measurements used, although all three techniques can use velocity, and the characteristics of the noise on the measurements of differences between the aligning INS and the reference. In quasi-stationary alignment, where zero velocity and angular rate with respect to the Earth are assumed, the main noise source is buffeting of the host vehicle by wind or human activity, such as fuelling or loading. In GNSS alignment, the GNSS receiver measurements are noisy. In transfer alignment, noise arises from flexure and vibration of the lever arm between the host vehicle's INS and the aligning INS.[*]

Most fine alignment algorithms operate on the basis that position, velocity, and attitude are roughly known at the start of the process. This is important for determining how the system errors vary with time and may allow simplifications, such as the small angle approximation, to be made. For some applications, such as GNSS alignment of a tactical-grade INS, there may be no prior knowledge of heading. However, GNSS and transfer alignment algorithms may be adapted to handle this as discussed in Section 14.4.4 [18].

The type of fine alignment technique that is most suitable depends on the application. When the INS is stationary on the ground, a quasi-stationary alignment is usually best as the noise levels are lowest. Where there is a choice between transfer alignment and GNSS alignment for in-flight applications, the best option is transfer alignment using an INS/GNSS reference, as this combines the higher short-term accuracy and update rate of the INS with the high long-term accuracy of GNSS.[†]

[*] This and subsequent paragraphs are based on material written by the author for QinetiQ, so comprise QinetiQ copyright material.

[†] End of QinetiQ copyright material.

Other navigation technology should be considered where neither GNSS nor transfer alignment is available.

5.7 INS Error Propagation

The errors in an inertial navigation system's position, velocity, and attitude solution arise from three sources. These are errors in the accelerometer and gyro measurements, initialization errors, and processing approximations. The latter includes approximations in the discrete-time navigation equations, the effects of finite iteration rates, gravity modeling approximations, computational rounding errors, and timing errors.

The navigation equations integrate the accelerometer and gyro biases to produce position, velocity, and attitude errors that grow with time. Similarly, the velocity initialization error is integrated to produce a growing position error. Random accelerometer and gyro noise and navigation equations limitations have a cumulative effect on the navigation solution errors. In addition, the attitude errors contribute to the velocity and position errors and there is both positive and negative feedback of the position errors through the gravity model.

INS error propagation is also affected by the host vehicle trajectory. For example, the effect of scale factor and cross-coupling errors depends on the host vehicle dynamics, as does the coupling of the attitude errors, particularly heading, into velocity and position.

Full determination of INS error propagation is a complex problem and is invariably studied using simulation software. A number of inertial navigation demonstrations with different grades of IMU are included in the MATLAB software on the accompanying CD. Here, a number of simple examples are presented to illustrate the main principles. These are divided into the short-term and the medium- and long-term cases, followed by a discussion of the effects of maneuvers on error propagation. A more detailed treatment of INS error propagation may be found in a number of inertial navigation texts [1, 11, 17].

Generally, an INS error is simply the difference between an INS-indicated quantity, denoted by a "~", and the true value of that quantity. Thus, the Cartesian position, velocity and acceleration errors are

$$\begin{aligned} \delta\mathbf{r}_{\beta\alpha}^{\gamma} &= \tilde{\mathbf{r}}_{\beta\alpha}^{\gamma} - \mathbf{r}_{\beta\alpha}^{\gamma} \\ \delta\mathbf{v}_{\beta\alpha}^{\gamma} &= \tilde{\mathbf{v}}_{\beta\alpha}^{\gamma} - \mathbf{v}_{\beta\alpha}^{\gamma} \\ \delta\mathbf{a}_{\beta\alpha}^{\gamma} &= \tilde{\mathbf{a}}_{\beta\alpha}^{\gamma} - \mathbf{a}_{\beta\alpha}^{\gamma} \end{aligned} . \tag{5.107}$$

Similarly, the latitude, longitude, and height errors are

$$\begin{aligned} \delta L_b &= \tilde{L}_b - L_b \\ \delta\lambda_b &= \tilde{\lambda}_b - \lambda_b \\ \delta h_b &= \tilde{h}_b - h_b \end{aligned} . \tag{5.108}$$

Coordinate transformation matrices should be used to calculate the attitude error. The coordinate transformation matrix form of the attitude error is defined by

$$\delta \mathbf{C}_{\beta}^{\alpha} = \tilde{\mathbf{C}}_{\beta}^{\alpha}\mathbf{C}_{\alpha}^{\beta}, \tag{5.109}$$

where the attitude error components are resolved about the axes of the α frame. This is because multiplying one coordinate transformation matrix by the transpose of another gives difference between the two attitudes that they represent. Note that

$$\begin{aligned} \delta \mathbf{C}_{\alpha}^{\beta} &= \tilde{\mathbf{C}}_{\alpha}^{\beta}\mathbf{C}_{\beta}^{\alpha} = \mathbf{C}_{\alpha}^{\beta}\left(\delta \mathbf{C}_{\beta}^{\alpha}\right)^{\mathrm{T}}\mathbf{C}_{\beta}^{\alpha} \\ \left(\delta \mathbf{C}_{\beta}^{\alpha}\right)^{\mathrm{T}} &= \mathbf{C}_{\beta}^{\alpha}\tilde{\mathbf{C}}_{\alpha}^{\beta} \end{aligned}, \tag{5.110}$$

where the components of $\delta \mathbf{C}_{\alpha}^{\beta}$ are resolved about the β frame axes.

Except under the small angle approximation, the attitude error in Euler angle form must be computed via coordinate transformation matrices (or quaternions or rotation vectors). When the small angle approximation applies, the attitude error may be expressed as a vector resolved about a chosen set of axes. $\delta \boldsymbol{\psi}_{\beta\alpha}^{\gamma}$ is the error in the INS indicated attitude of frame α with respect to frame β, resolved about the frame γ axes. From (2.26), the small angle attitude error may be expressed in terms of the coordinate transformation matrix form of the attitude error using

$$\left[\delta \boldsymbol{\psi}_{\beta\alpha}^{\alpha} \wedge\right] \approx \mathbf{I}_3 - \delta \mathbf{C}_{\beta}^{\alpha}, \qquad \left[\delta \boldsymbol{\psi}_{\beta\alpha}^{\beta} \wedge\right] \approx \delta \mathbf{C}_{\alpha}^{\beta} - \mathbf{I}_3. \tag{5.111}$$

Attitude errors are sometimes known as misalignments or misorientations. These terms are avoided here as they can be confused with the misalignments of the inertial-sensor sensitive axes with the body frame that produce cross-coupling errors (Section 4.4.2).

From Section 4.4.6, the accelerometer and gyro errors are [repeated from (4.18)]:

$$\begin{aligned} \delta \mathbf{f}_{ib}^{b} &= \tilde{\mathbf{f}}_{ib}^{b} - \mathbf{f}_{ib}^{b} \\ \delta \boldsymbol{\omega}_{ib}^{b} &= \tilde{\boldsymbol{\omega}}_{ib}^{b} - \boldsymbol{\omega}_{ib}^{b} \end{aligned}.$$

Simple models of gravity as a function only of latitude and height with few coefficients (see Section 2.4.7) are typically accurate to about 10^{-3} m s^{-2} (0.1 mg) in each direction [1, 17]. Consequently, they can be a significant source of error where higher precision inertial sensors are used.

The effect of timing errors is described in Section E.9 of Appendix E on the CD. Except for the highest precision applications, these errors are negligible compared to those arising from the inertial sensors.

5.7.1 Short-Term Straight-Line Error Propagation

The simplest INS error propagation scenario is short-term propagation when the host vehicle is traveling in a straight line at constant velocity and remains level. In considering only short-term error propagation, the effects of curvature and rotation of the Earth and gravity model feedback may be neglected, while there are no dynamics-induced errors where the host vehicle travels at constant velocity.

Figure 5.18 shows the position error growth with constant velocity, acceleration, attitude, and angular-rate errors. The position error is simply the integral of the velocity error, so with a constant velocity error,

$$\delta \mathbf{r}_{\beta b}^{\gamma}(t) = \delta \mathbf{v}_{\beta b}^{\gamma} t, \tag{5.112}$$

where β is the reference frame and γ the resolving axes. There is no error propagation between axes. As Figure 5.18 illustrates, an 0.1 m s^{-1} initial velocity error produces a 30-m position error after 300 seconds (5 minutes).

The velocity error is the integral of the acceleration error, so the following velocity and position errors result from a constant accelerometer bias:

$$\delta \mathbf{v}_{\beta b}^{\gamma}(t) \approx \mathbf{C}_b^{\gamma} \mathbf{b}_a t, \qquad \delta \mathbf{r}_{\beta b}^{\gamma}(t) \approx \tfrac{1}{2} \mathbf{C}_b^{\gamma} \mathbf{b}_a t^2. \tag{5.113}$$

There is no error propagation between axes where the attitude remains constant. As Figure 5.18 shows, an 0.01 m s^{-2} (~ 1 mg) accelerometer bias produces a 450-m position error after 300 seconds. Acceleration errors can also result from gravity modeling approximations, timing errors, and as a result of attitude errors.

Attitude errors produce errors in the transformation of the specific-force resolving axes from the body frame to an ECI, ECEF, or local-navigation frame, resulting

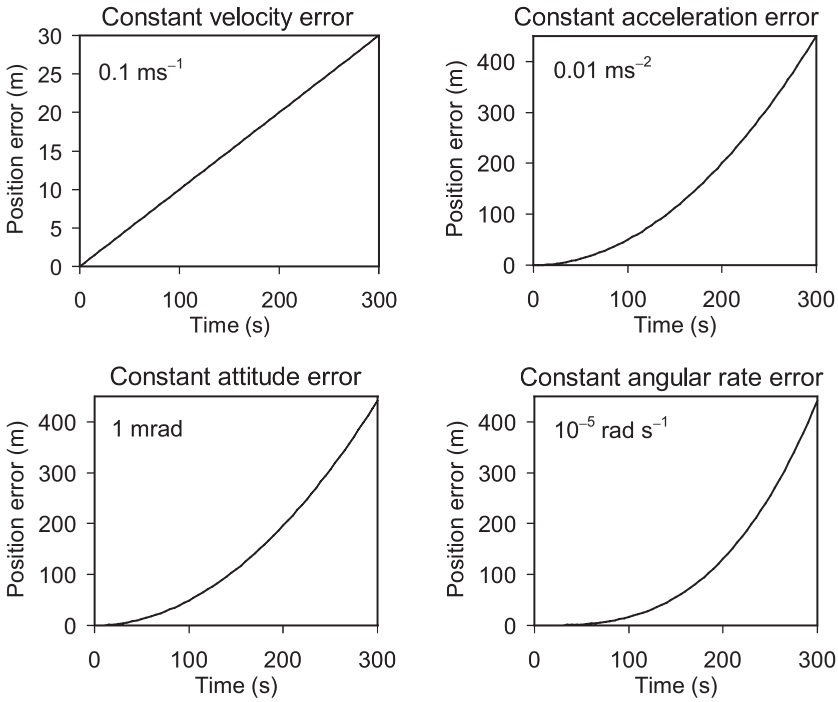

Figure 5.18 Short-term straight-line position error growth per axis for different error sources.

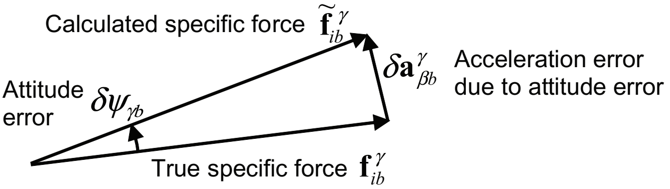
Calculated specific force $\tilde{\mathbf{f}}_{ib}^{\gamma}$
$\delta\mathbf{a}_{\beta b}^{\gamma}$ Acceleration error due to attitude error
Attitude error $\delta\psi_{\gamma b}$
True specific force $\mathbf{f}_{ib}^{\gamma}$

Figure 5.19 Acceleration error due to attitude error.

in errors in the acceleration resolved in that frame. Figure 5.19 illustrates this. When the attitude error may be expressed as a small angle, the resulting acceleration error is

$$\begin{aligned} \delta\mathbf{a}_{\beta b}^{\gamma}(t) &\approx \delta\boldsymbol{\psi}_{\gamma b}^{\gamma} \wedge \left(\mathbf{C}_b^{\gamma}\tilde{\mathbf{f}}_{ib}^{b}\right) \\ &= \mathbf{C}_b^{\gamma}\left(\delta\boldsymbol{\psi}_{\gamma b}^{b} \wedge \tilde{\mathbf{f}}_{ib}^{b}\right) \end{aligned}. \quad (5.114)$$

In the constant-velocity and level example, the specific force comprises only the reaction to gravity. Thus, pitch (body-frame y-axis) attitude errors couple into along-track (body-frame x-axis) acceleration errors and roll (body-frame x-axis) attitude errors couple into across-track (body-frame y-axis) acceleration errors. These acceleration errors are integrated to produce the following velocity and position errors.

$$\begin{aligned} \delta\mathbf{v}_{\beta b}^{\gamma}(t) &\approx \delta\boldsymbol{\psi}_{\gamma b}^{\gamma} \wedge \left[\mathbf{C}_b^{\gamma}\begin{pmatrix}0\\0\\-g\end{pmatrix}\right]t = \mathbf{C}_b^{\gamma}\left[\delta\boldsymbol{\psi}_{\gamma b}^{b} \wedge \begin{pmatrix}0\\0\\-g\end{pmatrix}\right]t \\ \delta\mathbf{r}_{\beta b}^{\gamma}(t) &\approx \tfrac{1}{2}\delta\boldsymbol{\psi}_{\gamma b}^{\gamma} \wedge \left[\mathbf{C}_b^{\gamma}\begin{pmatrix}0\\0\\-g\end{pmatrix}\right]t^2 = \tfrac{1}{2}\mathbf{C}_b^{\gamma}\left[\delta\boldsymbol{\psi}_{\gamma b}^{b} \wedge \begin{pmatrix}0\\0\\-g\end{pmatrix}\right]t^2 \end{aligned}. \quad (5.115)$$

As Figure 5.18 shows, a 1 mrad (0.057°) initial attitude error produces a position error of ~440m after 300 seconds.*

When the small angle approximation is valid, the attitude error due to a gyro bias, $\mathbf{b}_g$, is simply

$$\delta\boldsymbol{\psi}_{ib}^{b} \approx \mathbf{b}_g t. \quad (5.116)$$

This leads to velocity and position errors of

$$\delta\mathbf{v}_{\beta b}^{\gamma}(t) \approx \tfrac{1}{2}\mathbf{C}_b^{\gamma}\left[\mathbf{b}_g \wedge \begin{pmatrix}0\\0\\-g\end{pmatrix}\right]t^2, \qquad \delta\mathbf{r}_{\beta b}^{\gamma}(t) \approx \tfrac{1}{6}\mathbf{C}_b^{\gamma}\left[\mathbf{b}_g \wedge \begin{pmatrix}0\\0\\-g\end{pmatrix}\right]t^3. \quad (5.117)$$

As Figure 5.18 shows, a 10^{-5} rad s^{-1} (2.1 ° hr^{-1}) gyro bias produces a ~439m position error after 300 seconds.†

*This and subsequent paragraphs are based on material written by the author for QinetiQ, so comprise QinetiQ copyright material.

†End of QinetiQ copyright material.

The other major source of error in this scenario is noise. In a well-designed system, the inertial sensor noise will be the largest noise source and may be considered white over timescales exceeding one second. If the single-sided accelerometer noise PSD is S_a, then, from (B.113) and (B.116) in Appendix B on the CD, the standard deviations of the ensuing velocity and position errors are

$$\begin{aligned} \sigma\left(\delta v^{\gamma}_{\beta b,i}\right) &= \sqrt{S_a t} \qquad\qquad i \in x,y,z \\ \sigma\left(\delta r^{\gamma}_{\beta b,i}\right) &= \sqrt{\tfrac{1}{3} S_a t^3} \end{aligned} \quad . \tag{5.118}$$

Similarly, if the gyro noise PSDs is S_g, then, from (B.113) and (B.116) in Appendix B on the CD, the standard deviations of the ensuing attitude errors and horizontal position and velocity errors are

$$\begin{aligned} \sigma\left(\delta \psi^{\gamma}_{\beta b,i}\right) &= \sqrt{S_g t} \qquad\qquad i \in x,y,z \\ \sigma\left(\delta v^{n}_{\beta b,j}\right) &= g\sqrt{\tfrac{1}{3} S_g t^3} \qquad j \in N,E \, . \\ \sigma\left(\delta r^{n}_{\beta b,j}\right) &= g\sqrt{\tfrac{1}{5} S_g t^5} \end{aligned} \tag{5.119}$$

Figure 5.20 shows the growth in position error standard deviation due to sensor noise. If the accelerometer random noise PSD is 10^{-6} m^2 s^{-3} (corresponding to a root PSD of about 100 μg$\sqrt{\text{Hz}}$), the position error standard deviation after 300 seconds is 3m per axis. Similarly, if the gyro random noise PSD is 10^{-9} rad^2 s^{-1} (a root PSD of ~0.1 °/$\sqrt{\text{hr}}$), the position error standard deviation after 300 seconds is ~22m per horizontal axis.

Figure 5.21 shows the horizontal position error standard deviation growth using tactical-grade and aviation-grade INSs with the characteristics listed in Table 5.2. The tactical-grade INS error is more than an order of magnitude bigger than that of the aviation-grade INS after 300 seconds. The difference in horizontal and vertical performance of the tactical-grade INS arises because the gyro bias dominates and, under constant velocity conditions, this only affects horizontal navigation. For the aviation-grade INS, the acceleration, roll, and pitch errors dominate. Note that the initial position error has little impact after the first minute. Example 5.4 on the CD shows the calculations and can be edited using Microsoft Excel.

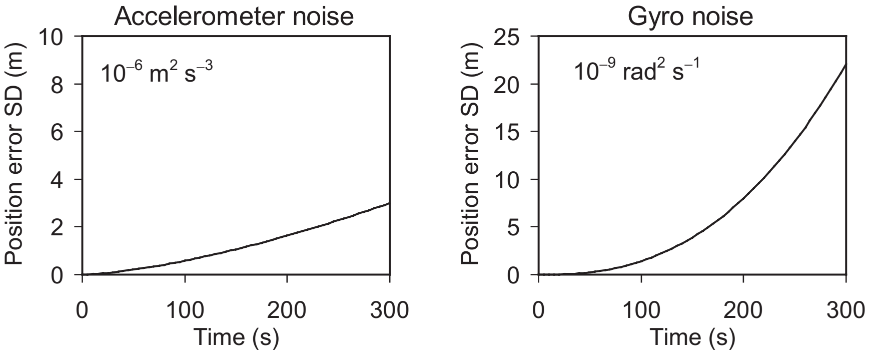

Figure 5.20 Short-term straight-line position error standard deviation growth per axis due to inertial sensor noise.

Table 5.2 Tactical-Grade and Aviation-Grade INS Characteristics

Sensor Grade	*Tactical*	*Aviation*
Initial position error standard deviation	10m	10m
Initial velocity error standard deviation	0.1 m s^{-1}	0.01 m s^{-1}
Initial (roll and pitch) attitude error standard deviation	1 mrad	0.1 mrad
Accelerometer bias standard deviation	0.01 m s^{-2} (1 mg)	0.001 m s^{-2} (0.1 mg)
Gyro bias standard deviation	5×10^{-5} rad s^{-1} (10 ° hr^{-1})	5×10^{-8} rad s^{-1} (0.01 ° hr^{-1})
Accelerometer noise PSD	10^{-6} m^2 s^{-3} (100 μg/√Hz)^2	10^{-7} m^2 s^{-3} (32 μg/√Hz)^2
Gyro noise PSD	10^{-9} rad^2 s^{-1} (0.1 °/√hr)^2	10^{-12} rad^2 s^{-1} (0.003 °/√hr)^2

The errors in Table 5.2 assume that no sensor calibration has been applied beyond that of the IMU manufacturer and that the roll and pitch have been initialized using a simple leveling procedure (see Section 5.6.2). Leveling correlates the roll and pitch errors with the accelerometer biases. Their effects on the velocity error largely cancel when the IMU orientation is the same as it was during leveling, reinforce when the IMU orientation is reversed within the horizontal plane, and are independent when the IMU is rotated by 90°. In Figure 5.21, the independent case is assumed.

Fine-alignment calibration (see Section 5.6.3 and Chapters 14 to 16) can significantly reduce the effective attitude errors and accelerometer and gyro biases. Figure 5.22 shows the horizontal position error standard deviation growth using a

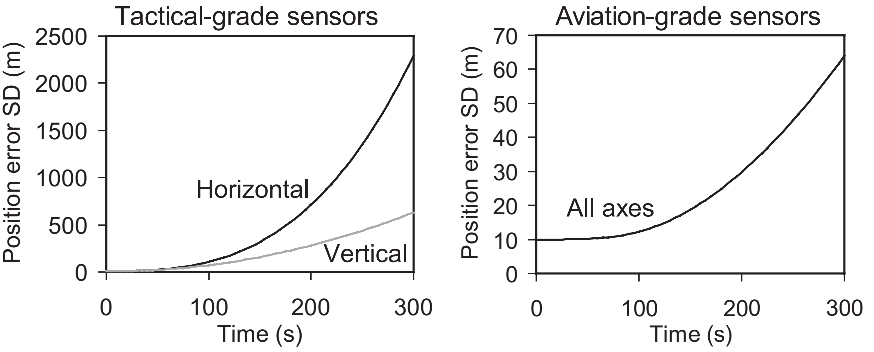

Figure 5.21 Short-term straight-line position error standard deviation growth per axis for tactical-grade and aviation-grade INSs.

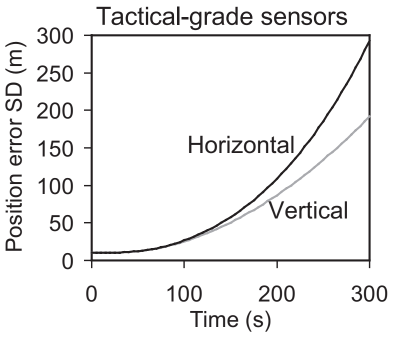

Figure 5.22 Short-term straight-line position error standard deviation growth per axis for a calibrated tactical-grade INS.

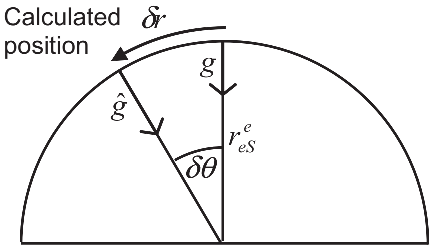

Figure 5.23 Gravity estimation from horizontal position error. (*From:* [9]. © 2002 QinetiQ Ltd. Reprinted with permission.)

calibrated tactical-grade INS where the residual roll and pitch errors are 0.3 mrad, the accelerometer biases 0.003 m s^{-2} (0.3 mg), and the gyro biases 5×10^{-6} rad s^{-1} (1 ° hr^{-1}). Comparing this with Figure 5.21, it can be seen that the calibration improves the position accuracy at 300 seconds by a factor of 8 horizontally and a factor of 3 vertically. This is also included in Example 5.4 on the CD.

5.7.2 Medium- and Long-Term Error Propagation

The gravity model within the inertial navigation equations, regardless of which coordinate frame they are mechanized in, acts to stabilize horizontal position errors and destabilize vertical channel errors.*

Consider a vehicle on the Earth's surface with a position error along that surface of δr_h. As a consequence, the gravity model assumes that gravity acts at an angle, $\delta\theta = \delta r / r_{eS}^{e}$, to its true direction, where r_{eS}^{e} is the geocentric radius. This is illustrated by Figure 5.23. Therefore, a false acceleration, $\delta\ddot{r}_h$, is sensed in the opposite direction to the position error. Thus, the horizontal position error is subject to negative feedback. Assuming the small angle approximation:

$$\delta\ddot{r}_h = -\frac{g}{r_{eS}^{e}}\delta r_h. \tag{5.120}$$

This is the equation for simple harmonic motion with angular frequency $\sqrt{g/r_{eS}^{e}}$. This is known as the Schuler frequency and the process is known as the Schuler oscillation. A pendulum with its pivot at the center of the Earth and its bob at the INS is known as a Schuler pendulum.† More generally, the Schuler frequency for a navigation system at any location is $\omega_s = \sqrt{g_b/r_{eb}^{e}}$. The corresponding period of the Schuler oscillation is

$$\tau_s = \frac{2\pi}{\omega_s} = 2\pi\sqrt{\frac{r_{eb}^{e}}{g_b}}. \tag{5.121}$$

As the strength of the gravity field and the distance from the INS to the center of the Earth varies with height and latitude, this period also varies. At the equator

*This and subsequent paragraphs are based on material written by the author for QinetiQ, so comprise QinetiQ copyright material.

†End of QinetiQ copyright material.

Table 5.3 Medium Term (Up to 4 Hours) Horizontal Position Error Growth from Selected Error Sources

Error Source	*North Position Error,* $\delta r^n_{eb,N}$	*East Position Error,* $\delta r^n_{eb,E}$
Initial velocity error, $\delta \mathbf{v}^n_{eb}$	$\frac{\sin \omega_s t}{\omega_s}\delta v^n_{eb,N}$	$\frac{\sin \omega_s t}{\omega_s}\delta v^n_{eb,E}$
Fixed accelerometer bias, $(\mathbf{C}^n_b \mathbf{b}_a)$	$\frac{1-\cos \omega_s t}{\omega_s^2}(\mathbf{C}^n_b \mathbf{b}_a)_N$	$\frac{1-\cos \omega_s t}{\omega_s^2}(\mathbf{C}^n_b \mathbf{b}_a)_E$
Initial attitude error, $\delta \boldsymbol{\psi}^n_{nb}$	$-(1-\cos \omega_s t) r^e_{eS} \delta \psi^n_{nb,E}$	$(1-\cos \omega_s t) r^e_{eS} \delta \psi^n_{nb,N}$
Fixed gyro bias, $(\mathbf{C}^n_b \mathbf{b}_g)$	$-\left(t-\frac{\sin \omega_s t}{\omega_s}\right) r^e_{eS}(\mathbf{C}^n_b \mathbf{b}_g)_E$	$\left(t-\frac{\sin \omega_s t}{\omega_s}\right) r^e_{eS}(\mathbf{C}^n_b \mathbf{b}_g)_N$

and at the Earth's surface, τ_s = 5,974 seconds (84.6 minutes). Consequently, over periods of order an hour, position errors arising from an initial velocity error, an initial attitude error, or an accelerometer bias are bounded and position errors arising from a gyro bias grow linearly with time, as opposed to cubicly. Table 5.3 gives the horizontal position errors arising from different sources for periods of up to about 4 hours [1]. Note that, in practice, instrument biases are not fixed with respect to the north and east axes.[‡]

Figure 5.24 shows the position error magnitude over a 6,000-second (100-minute) period arising from a 0.1 m s^{-1} initial velocity error, a 0.01 m s^{-2} acceleration error, a 1-mrad initial attitude error, and a 10^{-5} rad s^{-1} angular rate error. Note that the position error due to the gyro bias is not bounded in the same way as that due to the other error sources. Because of this, much more effort has gone into precision gyro development than precision accelerometer development. Thus, there is much greater variation in gyro performance across different grades of INS and IMU. Figure 5.25 shows the overall position error standard deviation over the same period for the aviation-grade INS specified in Table 5.2, neglecting the effects of sensor noise.

In practice, the position error growth will be much more complex than Figures 5.24 and 5.25 show, in which constant velocity is effectively assumed. Whenever the host vehicle changes direction, the direction of the accelerometer and gyro biases with respect to the north and east axes will change. This will reset the Schuler cycles for these errors with the cumulative velocity and attitude errors at this point acting as the initial velocity and attitude errors for the new Schuler cycle. This effect is known as Schuler pumping. Further Schuler cycles, which are added to the existing Schuler oscillation, arise from dynamics-induced velocity and attitude errors (see Section 5.7.3). The inertial sensor noise and vibration-induced noise also triggers a tiny additive Schuler cycle each time the navigation solution is updated. The cumulative effect of these errors can often exceed those of the initialization errors.

In closed-loop integrated navigation systems in which the inertial navigation solution is constantly corrected (see Section 14.1.1), the Schuler oscillation is largely irrelevant.

[‡] This paragraph, up to this point, is based on material written by the author for QinetiQ, so comprises QinetiQ copyright material.

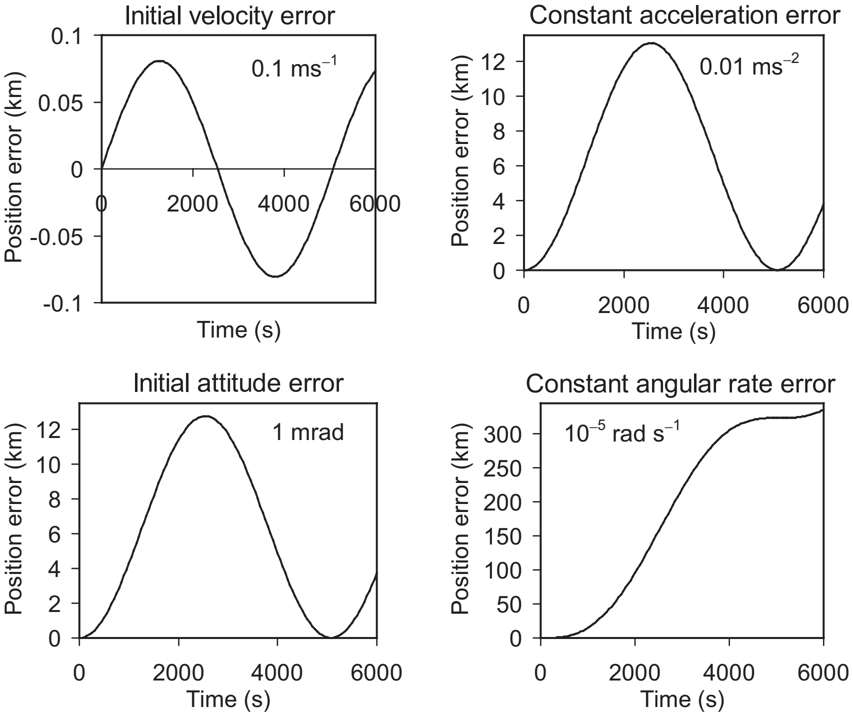

Figure 5.24 Horizontal position error growth per axis over a 6,000-second period for different error sources.

When the INS errors are resolved about the axes of an ECEF or local navigation frame, a further oscillation at the Earth rate, ω_{ie}, and amplitude modulation of the Schuler oscillation at angular frequency $\omega_{ie}\sin L_b$, known as the Foucault frequency, are seen. These are both due to feedback through the Coriolis force terms in the navigation equations. These oscillations are not observed in ECI-frame INS errors. However, they are present in an ECEF- or local-navigation-frame navigation solution converted from one computed in an ECI frame. Longer-term error propagation is discussed in more detail in [1, 15, 17].

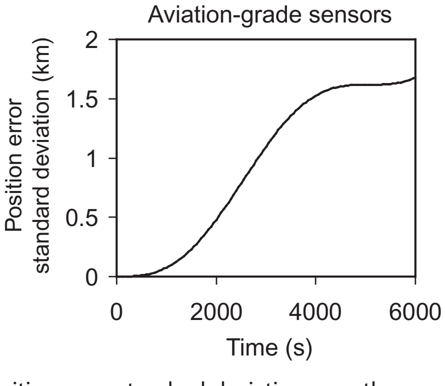

Figure 5.25 Horizontal position error standard deviation growth per axis over a 6,000-second period axis for an aviation-grade INS.

Considering now the vertical channel, as discussed in Section 2.4.7, the gravity varies with height approximately as[*]

$$g(h_b) \approx \left(1 - \frac{2h_b}{r_{eS}^e}\right) g_0. \tag{5.122}$$

A positive height error, δh_b, therefore leads to gravity being underestimated. As gravity acts in the direction opposite to that in which height is measured, the virtual acceleration that arises is in the same direction as the height error. Thus,[†]

$$\delta \ddot{h}_b \approx \frac{2g}{r_{eS}^e} \delta h_b. \tag{5.123}$$

Figure 5.26 shows the height error growth over 1,800 seconds arising from a 10-m initial height error and a 0.1 m s^{-1} initial vertical velocity error. The vertical position error is subject to positive feedback such that the height initialization error is doubled after ~750 seconds (12.5 minutes). Subsequent doublings occur after intervals of ~420 seconds (7 minutes). The height error growth due to the vertical velocity initialization error is more rapid. Consequently, an INS is only suited to long-term vertical navigation when it is aided by another navigation sensor.

For air applications, a barometric altimeter (baro) was always used for vertical aiding prior to the advent of GNSS and still forms a part of many integrated navigation systems. It measures the air pressure and then uses a standard atmospheric model to determine height. It exhibits errors that vary with the weather. A baro's operating principles and error sources are discussed in more detail in Section 6.2.1, while its integration with INS is described in Section 16.2.2.

For land and marine applications, it may be assumed that the average height above the terrain or sea surface is constant.

5.7.3 Maneuver-Dependent Errors

Much of the error propagation in inertial navigation depends on the maneuvers performed by the host vehicle. As discussed in Section 5.7.1, the effect of attitude errors on the velocity and position solutions depends on the specific force. At constant velocity, this is limited to the roll and pitch errors producing horizontal velocity errors. However, a linear acceleration or deceleration maneuver couples the heading error into the cross-track velocity and the pitch error into the vertical velocity. Similarly, a turn produces transverse acceleration, which couples the heading error into the along-track velocity and the roll error into the vertical velocity.

The heading error is typically an order of magnitude larger than the roll and pitch errors because heading is more difficult to align and calibrate (see Sections 5.6.2 and 14.2.1). Consequently, significant maneuvers can lead to rapid changes in velocity error. Consider the example of an aircraft flying north at 100 m s^{-1} with

[*] This and subsequent paragraphs are based on material written by the author for QinetiQ, so comprise QinetiQ copyright material.

[†] End of QinetiQ copyright material.

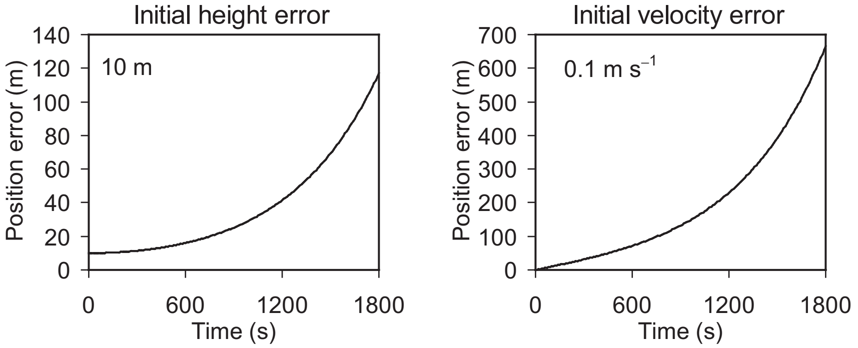

Figure 5.26 Vertical position error growth per axis over a 1,800-second period arising from height and velocity initialization errors.

north and east velocity errors of 0.05 m s^{-1} and 0.1 m s^{-1}, respectively, and a heading error of 1 mrad. The aircraft accelerates to 200 m s^{-1}, resulting in the east velocity error doubling to 0.2 m s^{-1}. It then undergoes a 90° turn to the west at constant speed; this maneuver increases the north velocity error to 0.25 m s^{-1} and drops the east velocity error to zero. Figure 5.27 illustrates this.

The effect of accelerometer and gyro scale factor and cross-coupling errors, gyro g-dependent errors, and higher-order inertial sensor errors (see Section 4.4) on navigation error growth also depends on the host vehicle maneuvers. In the previous example, a 500 ppm x-accelerometer scale factor error would produce an increase in north velocity error during the acceleration maneuver of 0.05 m s^{-1}, while a z-gyro scale factor error of –637 ppm would double the heading error to 2 mrad during the turn.

Velocity and direction changes often cancel out over successive maneuvers, so the effects of the scale factor and cross-coupling errors largely average out. An exception is circular and oval trajectories where the gyro scale factor and cross-coupling errors produce attitude errors that grow with time. The resulting velocity error will be oscillatory with the amplitude increasing with time, while the position error will be the sum of an oscillating term and a linear drift. Circling can occur when an aircraft

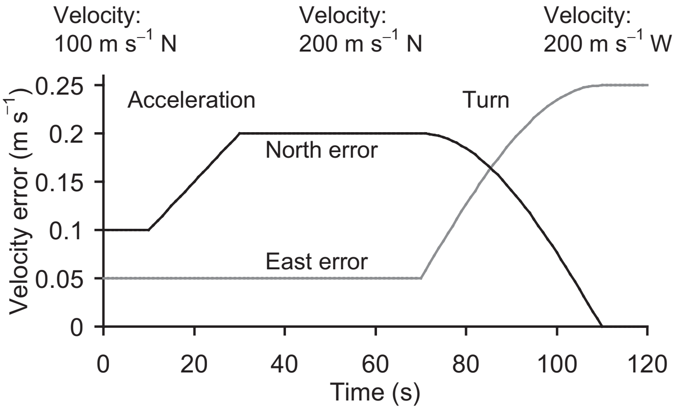

Figure 5.27 Illustration of the effect of maneuver on velocity error with a 1-mrad heading error.

is surveying an area or waiting in a holding pattern; it also occurs in motorsport. A similar problem occurs for guided weapons that spin about their roll axes.

Using tactical-grade gyros with scale factor and cross-coupling errors of around 300 ppm, the attitude errors will increase by about 0.1° per axis for each circuit completed by the host vehicle. With a circling period of 2 minutes, the position error will increase by about 400m per hour.

With a figure-of-eight trajectory, the attitude error due to gyro scale factor and cross-coupling errors will be oscillatory and correlated with the direction of travel. This produces a velocity error that increases with each circuit. Using tactical-grade gyros, position errors of several kilometers can build up over an hour.

5.8 Indexed IMU

In an *indexed* or *carouseling* IMU, the inertial sensor assembly is regularly rotated with respect to the casing, usually in increments of 90°. The rotation is typically performed about two axes or only about the vertical axis.

Indexing enables the cancellation over time of the position and velocity errors due to the accelerometer and gyro biases. The latter is particularly useful as gyro biases are the only major error source for which the horizontal position and velocity errors are not bounded over time by feedback through the gravity model (see Section 5.7.2). From (5.113) and (5.117), the growth in the position and velocity errors depends on the attitude of the IMU body frame with respect to the resolving axes of the navigation solution. Therefore, if the direction of an inertial sensor's sensitive axis is regularly reversed, its bias will lead to oscillatory position and velocity errors instead of continuously growing errors. To achieve this, it is rather more convenient to turn the inertial sensor assembly than to turn the entire host vehicle.

Single-axis indexing normally employs rotation of the inertial sensor assembly about the z-axis, generally the vertical. This enables cancellation of the effects of x- and y-axis accelerometer and gyro biases, but not the z-axis biases. The z-axis gyro bias has less impact on navigation accuracy as host-vehicle maneuvers are needed to couple the heading error into the position and velocity errors (see Section 5.7.3). The z-axis accelerometer bias mainly affects vertical positioning, which, as discussed in Section 5.7.2, always requires aiding from another sensor or a motion constraint, depending on the context. Dual-axis indexing enables cancellation of the effects of all six sensor biases on horizontal positioning [19].

Note that indexing does not cancel out the effects of gyro g-dependent biases, which are also not bounded by gravity-model feedback. Therefore, gyros that exhibit large g-dependent biases should be avoided in indexed IMUs.

The way in which the indexing rotations are performed is important. If all rotations about a given axis are performed in the same direction, the gyro scale-factor and cross-coupling errors will lead to continually increasing attitude errors. Thus, the rotations about a particular axis should average to zero over time. For dual-axis indexing, it is also important that the product of the rotations about any two axes also averages to zero over time.

The inertial sensor assembly of an indexed IMU will not generally be aligned with the host vehicle. The inertial navigation processor will compute the attitude of the inertial sensors with respect to the resolving frame. However, this is what it requires for positioning. The host vehicle attitude can be determined using the relative orientation of the sensor assembly, obtained from the indexing mechanism.

Indexed IMUs are typically deployed on submarines and military ships as these require the capability for stand-alone inertial navigation over many days and can handle the additional size, weight, and power consumption introduced by the indexing mechanism. However, rotation about the left-right axis may be used to limit the heading drift in foot-mounted inertial navigation [20].

5.9 Partial IMU

Normal land vehicle motion is subject to two motion constraints, also known as *nonholonomic constraints*. The velocity of the vehicle along the rotation axis of any of its wheels is zero. The velocity of the wheel rotation axes is also zero in the direction perpendicular to the road or rail surface. Note that, because of frame rotation, zero velocity does not necessarily imply zero acceleration. Consequently, under normal conditions (i.e., no wheel slip), the motion of a land vehicle has only four degrees of freedom, as opposed to six. By exploiting this context information, the vehicle motion can be measured using only four inertial sensors, known as a partial IMU. Vehicle motion in the presence of wheel slip is described in [21].

A common type of partial IMU has three accelerometers with mutually-perpendicular sensitive axes and a single gyro that measures the angular rate about the body z-axis, enabling changes in the vehicle heading to be measured. This is sometimes referred to as a 3A1G or 1G3A partial IMU. Partial IMU measurements are typically processed using conventional inertial navigation equations as described in Sections 5.2 to 5.5. The measurements from the missing inertial sensors are replaced with estimates, known as pseudo-measurements.

There are two main approaches to the generation of the pseudo-measurements and the application of the motion constraints. The first option is to simply assume the x- and y-axis angular rates are zero (i.e., $\omega_{ib,x}^{b} = \omega_{ib,y}^{b} = \alpha_{ib,x}^{b} = \alpha_{ib,y}^{b} = 0$). This will lead to errors in the position, velocity and attitude solution whenever the host vehicle pitches or rolls. These errors are then corrected by applying the motion constraints as Kalman filter measurement as described in Section 15.4.1 [22].

The second approach is to calculate the pseudo-measurements using the motion constraints and the remaining sensors. This is described in Section E.10 of Appendix E on the CD.

2A1G or 1G2A partial IMUs have also been proposed. These replace the z-axis accelerometer with a pseudo-measurement of $-g$, the reaction to gravity where that accelerometer is vertical [22]. However, even with the nonholonomic constraints, there is insufficient information to distinguish forward acceleration from changes in pitch. Consequently, sole-means navigation with such a sensor configuration requires a constant-gradient terrain along the direction of travel and external initialization of the pitch solution. In practice, 2A1G partial IMUs are only suitable for use in conjunction with other sensors, such as an odometer (Section 6.3), or GNSS (Chapters 8 to 10).

Problems and exercises for this chapter are on the accompanying CD.